Article

Cell

Inflammatory Cytokine TNFα Promotes the Long-Term Expansion of Primary Hepatocytes in 3D Culture

Graphical Abstract

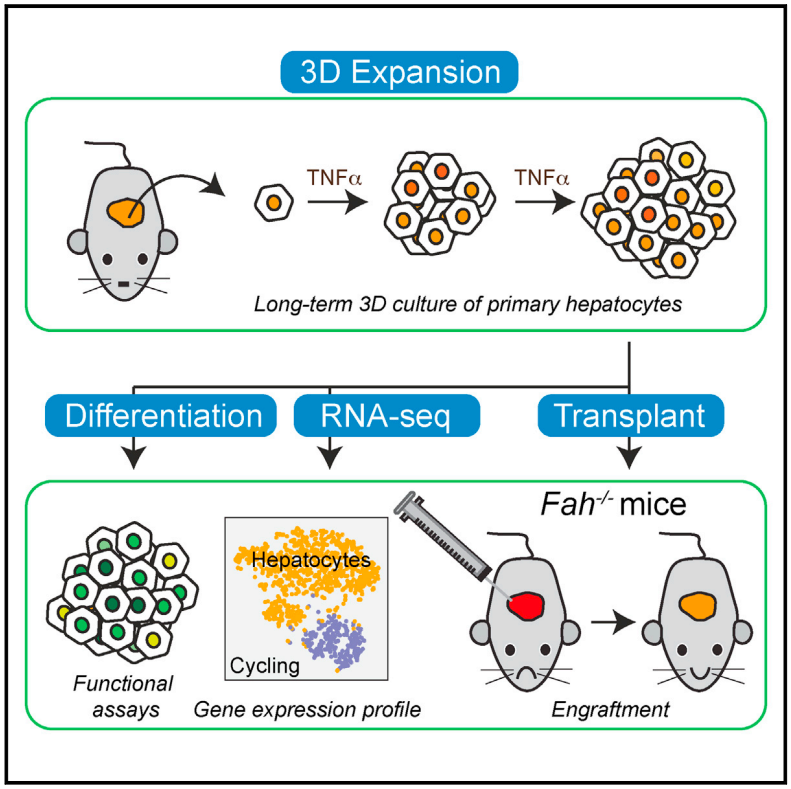

Authors

Weng Chuan Peng, Catriona Y. Logan, Matt Fish, ..., Markus Grompe, Bruce Wang, Roel Nusse

Correspondence

wcpeng@stanford.edu (W.C.P.), rnusse@stanford.edu (R.N.)

In Brief

The inflammatory cytokine TNFα enables the establishment of long-term 3D mouse organoid cultures from hepatocytes that are able to successfully engraft and repopulate damaged mouse livers.

Highlights

- Inflammatory cytokine TNFα promotes long-term expansion of primary hepatocytes
- 3D hepatocytes broadly express hepatocyte but not biliary markers
- 3D hepatocytes engraft and extensively repopulate the injured livers of *Fah*$^{-/-}$ mice
- Insights into tissue repair signals for the expansion of other primary cell types

Peng et al., 2018, Cell *175*, 1607–1619
November 29, 2018
https://doi.org/10.1016/j.cell.2018.11.012

CellPress

Cell

Inflammatory Cytokine TNFα Promotes the Long-Term Expansion of Primary Hepatocytes in 3D Culture

Weng Chuan Peng,[1,*] Catriona Y. Logan,[1] Matt Fish,[1] Teni Anbarchian,[1] Francis Aguisanda,[1] Adrián Álvarez-Varela,[1] Peng Wu,[1,3] Yinhua Jin,[1] Junjie Zhu,[4] Bin Li,[5] Markus Grompe,[5] Bruce Wang,[2] and Roel Nusse[1,6,*]

[1]Howard Hughes Medical Institute, Department of Developmental Biology, Institute for Stem Cell Biology and Regenerative Medicine, Stanford University School of Medicine, Stanford, CA 94305, USA

[2]Department of Medicine and Liver Center, University of California, San Francisco, San Francisco, CA 94143, USA

[3]Department of Pediatrics, Stanford University School of Medicine, Stanford, CA 94305, USA

[4]Department of Electrical Engineering, Stanford University, Stanford, CA 94305, USA

[5]Oregon Stem Cell Center, Oregon Health and Science University, Portland, OR 97239, USA

[6]Lead Contact

*Correspondence: wcpeng@stanford.edu (W.C.P.), rnusse@stanford.edu (R.N.)

https://doi.org/10.1016/j.cell.2018.11.012

SUMMARY

In the healthy adult liver, most hepatocytes proliferate minimally. However, upon physical or chemical injury to the liver, hepatocytes proliferate extensively *in vivo* under the direction of multiple extracellular cues, including Wnt and pro-inflammatory signals. Currently, liver organoids can be generated readily *in vitro* from bile-duct epithelial cells, but not hepatocytes. Here, we show that TNFα, an injury-induced inflammatory cytokine, promotes the expansion of hepatocytes in 3D culture and enables serial passaging and long-term culture for more than 6 months. Single-cell RNA sequencing reveals broad expression of hepatocyte markers. Strikingly, *in vitro*-expanded hepatocytes engrafted, and significantly repopulated, the injured livers of *Fah*$^{-/-}$ mice. We anticipate that tissue repair signals can be harnessed to promote the expansion of otherwise hard-to-culture cell-types, with broad implications.

INTRODUCTION

The capacity to stably expand healthy, non-transformed cell types *in vitro* would abundantly supply cells for regenerative therapies and provide ample material for basic biological studies. However, it is generally accepted that the majority of adult primary cell types are refractory to *in vitro* expansion, perhaps because they divide infrequently *in vivo*. For example, the liver—the focus of this study—is generally subject to a low turnover rate during homeostasis (Magami et al., 2002). The liver parenchyma comprises two major cell types: hepatocytes (~80%) and bile-duct epithelial cells (BECs, ~20%). BECs are responsible for bile-acid transport, whereas hepatocytes execute varied functions including metabolism, detoxification, and protein production (Halpern et al., 2017; Miyajima et al., 2014). Moreover, hepatocytes are diverse, and their function and gene expression differ depending on their location within the liver lobule (the functional unit of the liver), which is organized along a spatial axis spanning from the central vein (CV) to the portal vein (PV) (Kietzmann, 2017). Along the CV-PV axis, hepatocytes are heterogeneous: *Axin2*$^{+}$ pericentral hepatocytes residing next to the CV express various cytochrome enzymes and proliferate during homeostasis, ultimately replacing ~20%–30% of hepatocytes across the lobule over 1 year, as shown by lineage tracing (Wang et al., 2015). They divide under the influence of WNT and RSPO3 signals secreted by CV endothelial cells (Wang et al., 2015). Separately, rare *Telomerase*-expressing hepatocytes scattered throughout the liver lobule also proliferate and generate small clones after long-term lineage tracing (Lin et al., 2018). However, taken as a whole, hepatocytes generally divide slowly by comparison to fast-cycling tissues such as the small intestine, which renews itself every 3–5 days (Clevers et al., 2014).

In contrast to the resting liver, hepatocyte proliferation increases dramatically after physical or chemical damage. A hallmark of the liver is its capacity to regenerate following injury: even after surgical removal of two-thirds of its mass (partial hepatectomy [PH]), it can regenerate to its original size in 5–7 days (Michalopoulos and DeFrances, 1997). The usually quiescent mature hepatocytes enter an intense phase of DNA synthesis under the direction of injury-invoked regenerative signals that have been well documented (Kang et al., 2012; Michalopoulos, 2007). For instance, Kupffer cells (liver-resident macrophages) secrete inflammatory cytokines such as interleukin (IL)-6 and tumor necrosis factor (TNF)-α, which are crucial early signals that initiate regeneration (Michalopoulos, 2007). Plasma levels of hepatocyte growth factor (HGF) and epidermal growth factor (EGF) increase quickly following PH, functioning as potent mitogenic factors that stimulate DNA synthesis in hepatocytes (Lindroos et al., 1991; Skov Olsen et al., 1988). In addition, hepatocytes themselves secrete growth factors required for angiogenesis that include VEGF, FGF1, and TGFα (Michalopoulos, 2007). Non-parenchymal cells, such as stellate cells and endothelial cells, also contribute to liver regeneration. For example, stellate cells secrete HGF and norepinephrine, while endothelial cells secrete HGF and heparin binding-EGF (Michalopoulos, 2007).

Corroborating the importance of these pro-inflammatory signals in liver regeneration, TNF receptor (TNFR) 1 or IL-6 knockout mice show impaired DNA synthesis after PH (Cressman et al., 1996; Yamada et al., 1997), and blocking TNFα with antibodies inhibits liver regeneration after PH (Akerman et al., 1992). Collectively, these studies demonstrate that inflammatory cytokines and growth factors are critical for tissue regeneration and restoration of liver function.

The liver is not the only organ that relies on inflammatory signals for regeneration after injury. Indeed, inflammation and regeneration are closely linked across multiple tissues such as the skeletal muscle, intestine, colon, hair follicles, skin, and central nervous system (Aurora and Olson, 2014; Karin and Clevers, 2016). The inflammatory cytokines IL-6, TNFα, and their related family members activate a series of transcription factors that include NF-κB, JAK/Stat, AP-1, and YAP (Karin and Clevers, 2016). These inflammatory signals in turn enhance cellular proliferation by promoting cell-cycle entry (Karin and Clevers, 2016). In particular, excessive activation of NF-κB signaling is linked to tumor initiation in the intestine and hepatocellular carcinoma in the liver, suggestive of a more general role in cell-cycle regulation (Karin and Greten, 2005; Oguma et al., 2008; Pikarsky et al., 2004; Schwitalla et al., 2013). Such observations led us to postulate that regenerative cytokines could be harnessed beyond the context of injury to expand otherwise-hard-to-expand primary cell types *in vitro*.

It has been challenging to culture and stably expand hepatocytes. Currently, liver organoids can only be generated from BECs and "tumoroids" that are formed from primary liver cancer cells (Broutier et al., 2016, 2017; Huch et al., 2013, 2015). Signals that are widely employed in prevailing organoid methods (Huch and Koo, 2015) or two-dimensional (2D) culture (Katsuda et al., 2017) fail to expand primary hepatocytes in three-dimensional (3D) culture. Given the role of inflammatory cytokines in tissue repair, we asked whether such signals could be employed to expand hepatocytes *in vitro*. Here, we find that the inflammatory signal TNFα enables the *in vitro* expansion of primary mouse hepatocytes in 3D culture, which broadly express markers of hepatocytes but not other cell types, as revealed by single-cell RNA sequencing (RNA-seq). Importantly, cultured hepatocytes can engraft the injured livers of *Fah*$^{-/-}$ mice and robustly regenerate liver tissue *in vivo*.

RESULTS

TNFα Promotes the Expansion of Primary Hepatocytes in 3D Culture

We first attempted to culture hepatocytes in 3D Matrigel droplets overlaid by culture media supplemented with EGF, HGF, and the WNT agonist CHIR 99021 (see STAR Methods). However, only a few colonies were observed after 2 weeks in culture (Figures 1A and 1B). Lipid droplets, which are frequently associated with cellular stress and impaired regeneration (Lee et al., 2015; Michalopoulos, 2007; Torbenson et al., 2002), were detected in many hepatocytes (Figure S1A). Most cells eventually deteriorated within the first 2–3 weeks of culture or after the first passage (Figure 1C).

TNFα is a pro-inflammatory signal critical for fetal liver growth and liver regeneration after injury (Beg et al., 1995; Kirillova et al., 1999; Yamada et al., 1997, 1998). We asked whether TNFα could be used to expand hepatocytes *in vitro*. Strikingly, in the presence of TNFα, hepatocyte colony formation was observed in the first 2 weeks of culture, with colony-forming efficiencies of up to 15% (i.e., 150 colonies formed per 1,000 primary hepatocytes seeded; Figures 1A and 1B). The colonies were mostly comprised of cells with single large nuclei and scant cytoplasm, and some colonies were more than 100 μm in size (Figure S1B). To test whether TNFα was continuously required for both the initiation as well as maintenance of colonies, TNFα was removed from the culture media after passaging (Figure 1C). We used Hoechst intensity as a measure of colony expansion. When TNFα was withdrawn after passaging, colonies showed a minimal increase in DNA content when compared to culture with TNFα (Figure 1D) and accumulated lipid droplets massively, which were visible under phase-contrast or by LipidTOX staining, and many colonies eventually deteriorated in culture (Figures 1C and S1C). When TNFα was withdrawn at later passages, a similar outcome was observed (Figures 1D and S1D).

TNFα has been shown to induce DNA replication in hepatocytes through NF-κB signaling (Kirillova et al., 1999; Webber et al., 1998; Wullaert et al., 2007). To test whether NF-κB signaling is required for the expansion of hepatocytes in culture, we blocked NF-κB signaling using the specific ATP-competitive IKK-β inhibitor ML120B. Indeed, blockade of NF-κB signaling reduced the number of colonies (Figure S1E). Finally, another inflammatory cytokine critical for liver regeneration, IL-6, did not replace the role of TNFα in hepatocyte expansion, with most cells deteriorating after the first 3 weeks in culture (Figure S1F). Taken together, TNFα-containing culture conditions consistently allowed for serial passaging and expansion of hepatocyte colonies for multiple months in a TNFα-dependent manner, with the longest culture currently at 8 months (Figures 1E and S1G).

Characterization of Hepatocyte Cultures

3D hepatocyte colonies derived in our culture media were morphologically distinct from liver organoids previously derived from BECs (Huch et al., 2013, 2015). In our hepatocyte colonies, polygonal cells were tightly packed in compact 3D structures, with larger colonies organized with pseudo-glandular rosettes containing occasional lumen-like structures (Figures 2A and S2A). Immunofluorescence revealed broad expression of the general hepatocyte marker HNF4α, with CD26^{+} bile canaliculi structures located centrally, reminiscent of structural polarity typically present in the liver lobule (Figure 2A). YAP and NF-κB, transcription factors important for liver regeneration after injury, were localized to the nuclei (Su et al., 2015; Yimlamai et al., 2014). In addition, the proliferation marker KI67 was detected, and mitotic cells could be observed by Hoechst staining (Figures 2A and S2A).

During liver regeneration, progenitor markers are often transiently upregulated, while differentiation-associated genes are downregulated (Karin and Clevers, 2016; Michalopoulos and DeFrances, 1997; Su et al., 2015). Quantitative PCR (qPCR) revealed that cultured hepatocytes expressed genes associated with hepatocyte functions such as *Alb*, *Ttr*, *Tat*, and *Fah*, albeit at

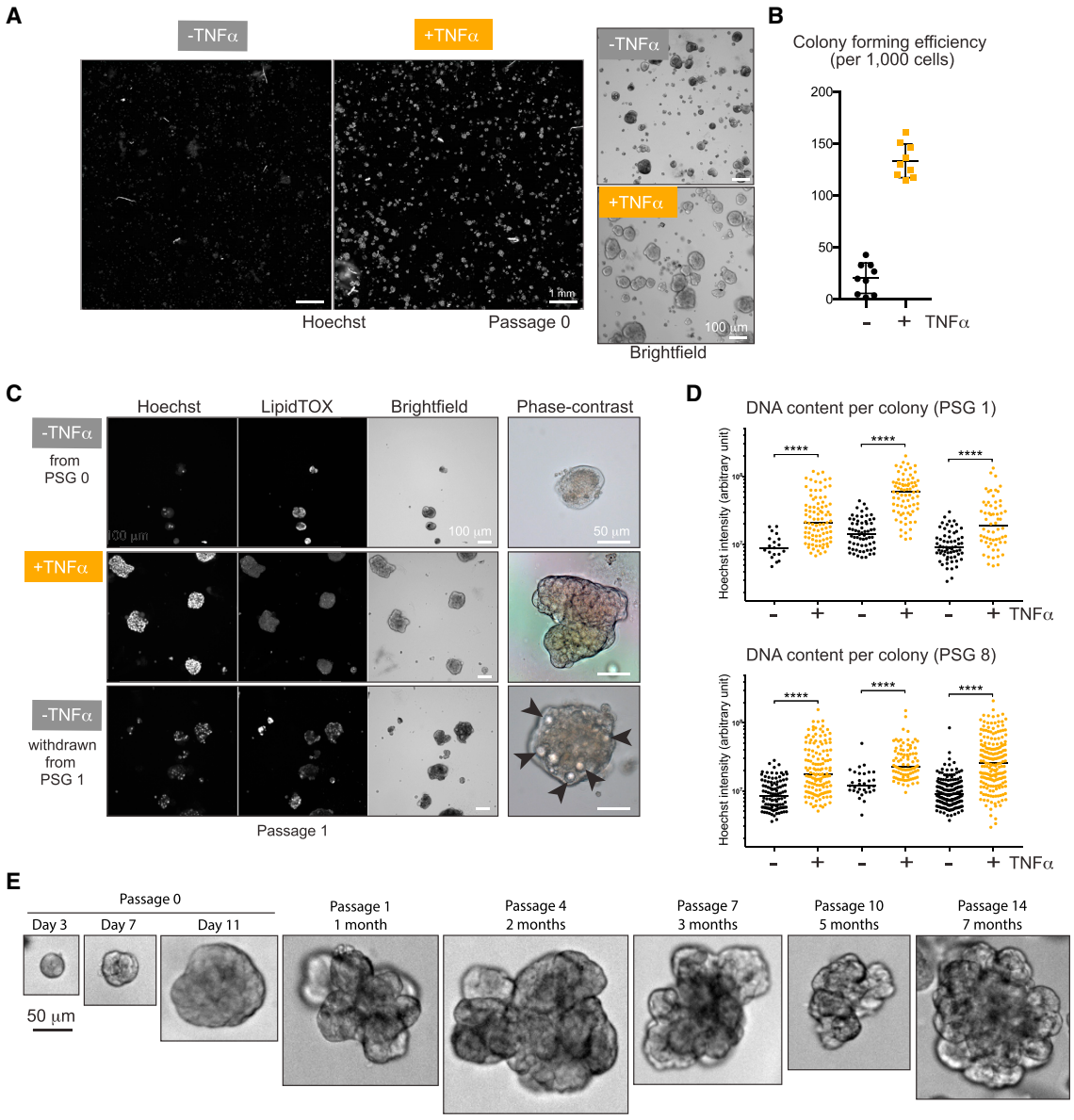

Figure 1. TNFα Promotes the Expansion of Primary Hepatocytes in 3D Culture

(A) Confocal montage and brightfield images of freshly isolated primary mouse hepatocytes cultured in expansion media, with or without TNFα for 2 weeks. Nuclei were counterstained with Hoechst and shown on the same intensity scale.

(B) Colony-forming efficiency of hepatocytes cultured with or without TNFα. Approximately 1,000 cells were seeded, and colony counts were performed after 2 weeks. Individual data points, mean and SD are shown, n = 3 biological replicates.

(C) Images of hepatocyte cultures at passage 1. Cells cultured continuously without TNFα (top), with TNFα (middle), or with TNFα withdrawn after passaging (bottom). Nuclei (Hoechst), lipid droplets (LipidTOX), and brightfield images are shown. Phase-contrast images highlight lipid droplets (arrowheads).

(D) Scatterplots showing Hoechst intensity per hepatocyte colony. Hepatocytes were cultured continuously with TNFα or with TNFα withdrawn from culture media at passage 1 (top) or at passage 8 (bottom). All measurements were performed at least 1 week after TNFα withdrawal. Each dot represents a colony, individual data points and medians for each biological replicate are shown, Mann-Whitney U test, ****$p < 0.0001$.

(E) Representative images of long-term cultured hepatocytes in the presence of TNFα.

levels slightly lower than in freshly isolated primary hepatocytes (Figures 2B and S2B). Periportal genes such as *Cps1* and *Cyp2f2* were strongly downregulated, presumably due to the Wnt activator present in the expansion medium, as Wnt is known to suppress periportal genes *in vivo* (Benhamouche et al., 2006; Planas-Paz et al., 2016; Rocha et al., 2015) (Figure 2B). Other cytochrome enzymes expressed in the pericentral zone, such as *Cyp1a2* and *Cyp3a11*, were also markedly reduced (Figure 2B).

Next, we tested whether expression of hepatocyte functional genes could be induced in culture in the absence of TNFα and in the presence of factors that promote maturation, such as dexamethasone (DEX) (Michalopoulos et al., 2003). We used

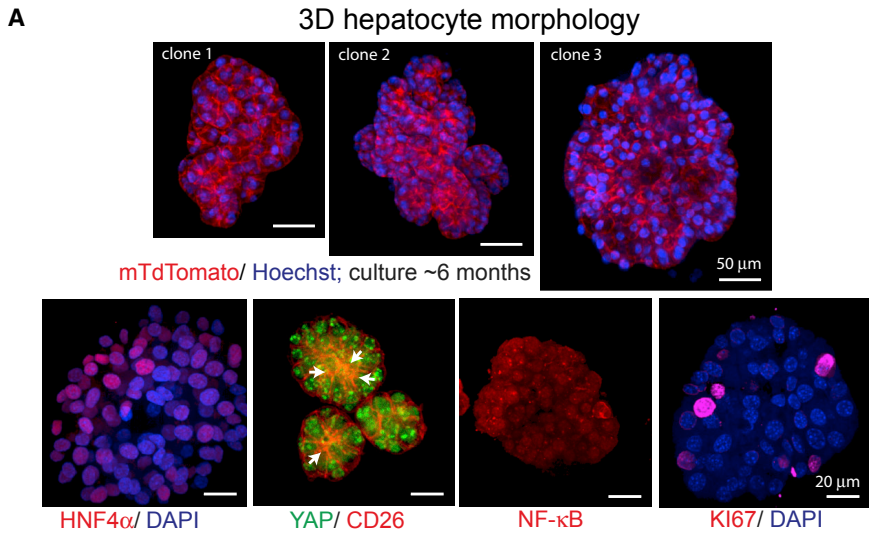

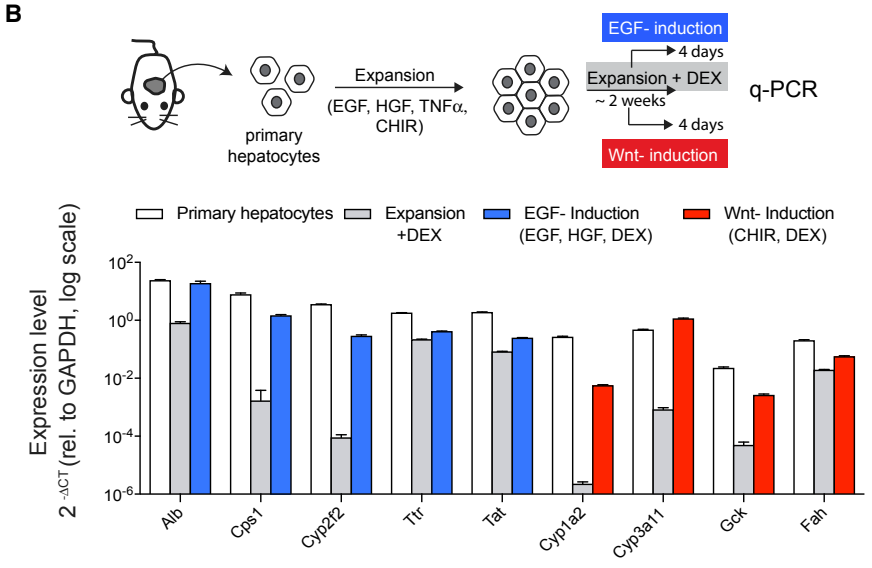

Figure 2. Expression and Modulation of Functional Markers in 3D Hepatocytes

(A) Confocal images of hepatocyte colonies constitutively expressing membrane TdTomato (top) or stained for markers indicated and visualized by immunofluorescence (bottom). Arrows mark CD26+ bile canaliculi. Scale bars, 50 μm (top), 20 μm (bottom).

(B) Schematic diagram of the experimental strategy (top) for gene expression analysis of freshly isolated primary hepatocytes and cultured hepatocytes by qPCR. Data are represented as mean and SD of three measurements (bottom). See also Figure S2.

two different strategies to separately induce expression of pericentral and periportal genes, as such genes are usually induced by mutually exclusive signals *in vivo*: Wnt signaling has been shown to promote pericentral, and inhibit periportal, gene expression, while Ras signaling promotes periportal gene expression (Benhamouche et al., 2006; Hailfinger et al., 2006; Halpern et al., 2017; Planas-Paz et al., 2016; Rocha et al., 2015). To induce periportal gene expression, cultured cells were switched to induction medium for 4 days, in which EGF and HGF were maintained in the medium while CHIR and TNFα were withdrawn (Figures 2B and S2B). The expression of *Alb* increased to a level comparable to primary hepatocytes, and *Cps1* and *Cyp2f2* were strongly upregulated (Figure 2B). Separately, to promote the expression of pericentral genes, the Wnt agonist CHIR was maintained while EGF, HGF, and TNFα were withdrawn from the media. In this setting, the expression levels of *Cyp1a2*, *Cyp3a11*, and *Gck* were upregulated (Figure 2B).

We performed functional assays to further characterize the 3D hepatocyte cultures. First, cultured hepatocytes secreted high levels of albumin protein into the media, with higher levels of albumin detected in EGF-induction medium than expansion medium (Figure 3A), consistent with qPCR data. Second, hepatocytes cultured in EGF medium displayed higher levels of CYP3A11 (the ortholog of human CYP3A4) enzymatic activity than hepatocytes cultured in expansion media and, unexpectedly, also Wnt-induction media. (Figure 3A). In both assays, the trend is maintained in 3- to 7- month cultures, indicating that functional properties are retained in long-term culture. Third, cultured hepatocytes could uptake fluorescently conjugated low-density lipoprotein (LDL) (Figure 3B). Fourth, the addition of fluorescein diacetate dye led to its rapid uptake and accumulation in the bile canaliculi structures and lumens between cells (Figures 3C and S3A), reflecting functional bile canaliculi. Fifth, hepatocytes could store glycogen, as detected by periodic acid-Schiff (PAS) staining (Figure 3D). In addition, cultured hepatocytes could be genetically manipulated, as shown by lentiviral transduction of *GFP* (Figures 3E and S3B). Further, 3D hepatocytes could be co-cultured with human umbilical vein endothelial cells (HUVECs). 3D hepatocyte-HUVEC aggregates were observed 2 days after the initiation of co-culture, and larger aggregates could be observed 2 weeks later (Figures 3F and S3C).

Single-Cell Transcriptome Analysis Reveals Expression of Hepatocyte and Proliferation Markers in Expansion Medium and Upregulation of Functional Markers in Induction Medium

To evaluate the gene expression profile of, and heterogeneity among, single hepatocytes after *in vitro* expansion, we performed single-cell RNA-seq using the 10x Genomics Chromium system (Zheng et al., 2017). We performed single-cell RNA-seq

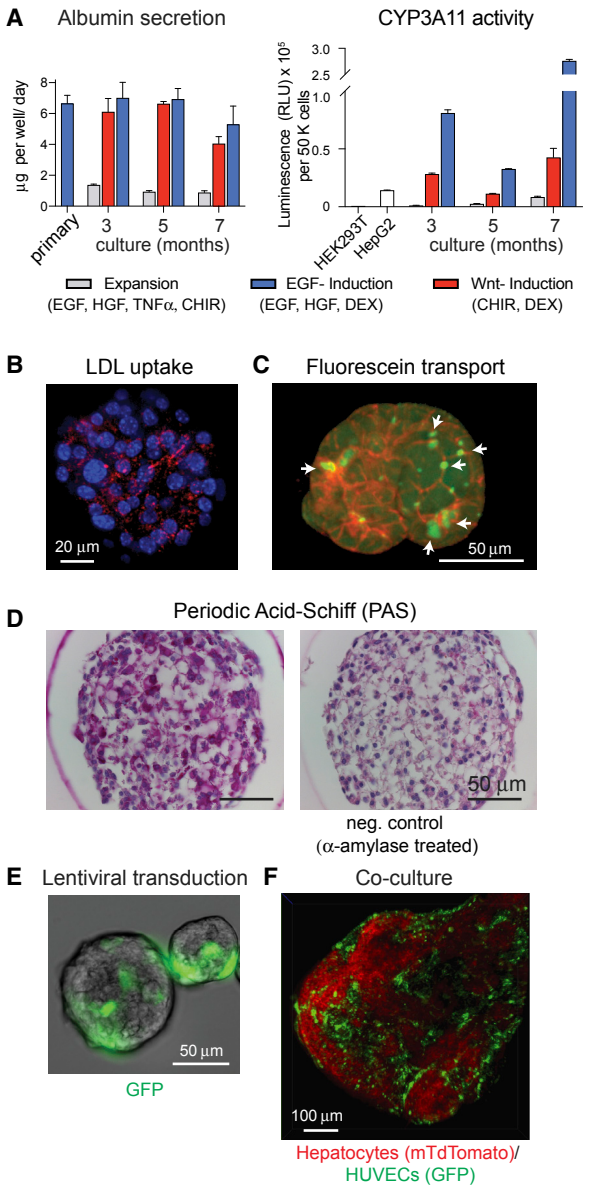

Figure 3. 3D Hepatocytes Display Functional Activities

(A) Albumin secretion measured by mouse albumin enzyme-linked immunosorbent assay (ELISA) kit (left) and CYP3A11 activity measured by P450-Glo CYP3A4 assay using luciferin-IPA as a substrate (right). Data are represented as mean and SD of three measurements.

(B) LDL uptake visualized by DyLight-550-conjugated LDL (red). Nuclei were counterstained with Hoechst (blue).

(C) Accumulation of fluorescein diacetate (green) in the bile canaliculi structures (arrows). Red, membrane TdTomato.

(D) Glycogen storage visualized by PAS staining.

(E) Overlay of wide-field fluorescence and brightfield images of 3D hepatocytes expressing GFP (green) introduced by lentiviral transduction.

(F) Confocal z stack projection of aggregates of 3D hepatocytes constitutively expressing membrane TdTomato (red) and HUVECs constitutively expressing GFP (green), 2 weeks after the initiation of co-culture.

on 1,192 hepatocytes (derived from one male and one female) cultured in expansion medium and jointly analyzed these data by principal component analysis (PCA). The top ten principal components were used for clustering analysis (Butler et al., 2018), and the resulting clusters were visualized in t-distributed stochastic neighbor embedding (t-SNE) projections (Figure 4A).

Hepatocyte markers such as *Alb*, *Apoa1*, *Ttr*, *Serpina1c*, *Hnf4a*, *Fga*, *Fn1*, *Rbp4*, *Glul*, and *Slc1a2* were broadly and heterogeneously expressed across the entire population of cultured hepatocytes (Figure 4B). Gene ontology (GO) analysis of the most abundantly expressed genes revealed an enrichment of relevant functional categories, including cytolysis, lipoprotein particle remodeling, blood coagulation, retinol metabolic process, regulation of G1/S phase transition, and response to tumor necrosis factor (Figure S4). Crucially, canonical biliary markers such as *Epcam*, *Krt7*, *Krt19*, *Aqp1*, *Aqp4*, and *Cldn7* were present at low levels or not detected (Figure 4C, in red, and data not shown). On the contrary, hepatocyte epithelial markers such as *Krt8*, *Krt18*, and *Tjp1* (*Cd26*) were highly expressed in many cells (Figure 4C, in red, and data not shown), suggesting that the vast majority of cultured cells are hepatocytes, without evidence for a distinct subset of non-hepatocyte cells.

Clustering analyses of the entire population of cultured hepatocytes (Figure 4A) revealed a subset of cells (259 out of 1,192 cells) that expressed proliferation markers such as *Ccna2*, *Top2a*, *Mki67*, *Cdk1*, and *Cenpm* (Figures 4D and S4A). GO analysis of genes differentially expressed by this putative cluster of proliferating cells confirmed enrichment for terms such as mitosis, cell-cycle regulation, chromosome segregation, chromatin remodeling, and DNA replication (Figure S4B). We thus assigned this subset of cells as cycling hepatocytes. The distinction between cycling versus non-cycling cells was also clearly captured by PC2 (Figure 4A). Of note, cells from male and female samples were similarly represented in the cycling and non-cycling hepatocytes; a small subset of female hepatocytes also formed a distinct cluster from the remaining hepatocytes (Figure 4A).

A key question is whether *in vitro*-expanded hepatocytes transcriptionally resemble primary hepatocytes. To this end, we compared the expression profile of expanded hepatocytes to freshly isolated primary hepatocytes (1,233 cells derived from 3-month-old mice), described previously (Tabula Muris Consortium et al., 2018) (Figure 5A). Genes associated with inflammatory responses typically showed little to no expression in primary hepatocytes but were detected in cultured hepatocytes (Figure S5A), such as acute phase proteins serum amyloid A3, *Saa3* (and *Saa1*, *Saa2*), lipocalin 2 (*Lcn2*), haptoglobin (*Hp*), and clusterin (*Clu*) (Figure 5B). Acute phase proteins are usually expressed during inflammation to promote clearance of pathogens and to limit excessive inflammatory responses (Robinson et al., 2016). For instance, *Lcn2* has been shown to exert protective effects against cytokine-induced stress during acute liver injury (Borkham-Kamphorst et al., 2013; Hu et al., 2015). Further, cytokines and chemokines (*Ccl20*, *Ccl2*, *Cxcl1*, *Cxcl5*), many of which are induced by TNFα or interleukins, were highly expressed in culture but notably absent in primary hepatocytes (Figure 5B).

Next, we examined the expression of regenerative factors that have been previously described to be critical for liver regeneration after partial hepatectomy (Costa et al., 2003; Karin and

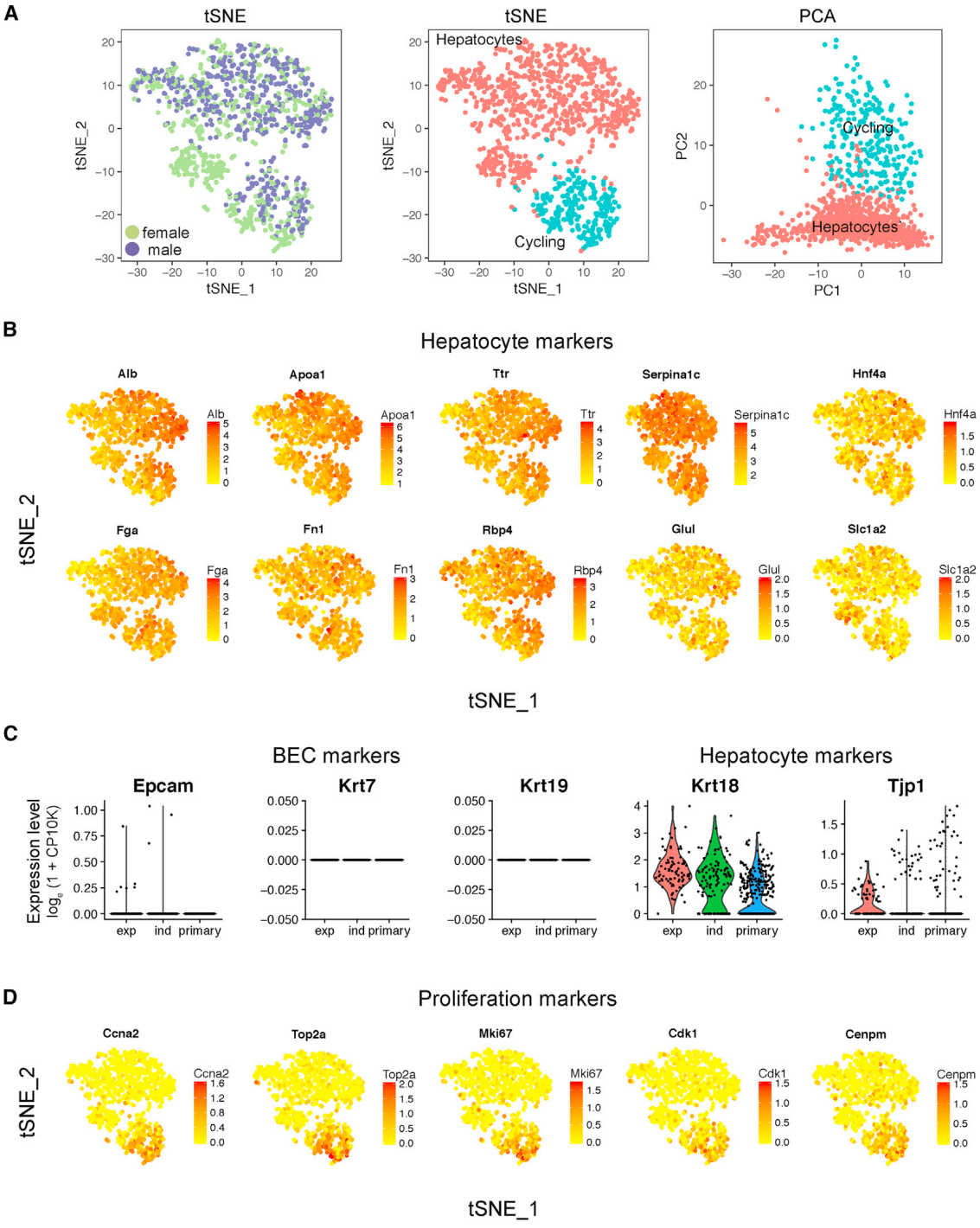

Figure 4. Single-Cell RNA-Seq Reveals Broad Expression of Hepatocyte Markers and the Presence of a Subset of Cycling Cells

(A) t-SNE projection of expanded hepatocytes (n = 1,192 cells) labeled by sex (left) or cycling state (middle) and the projection of the same cells onto the first two principal components (right).

(B) t-SNE plots indicating the expression of representative hepatocyte markers.

(C) Violin plots showing the expression of representative hepatocyte markers and the absence of biliary markers. Exp, expansion medium; ind, EGF-induction medium; primary, primary hepatocytes; n = subset of 100 cells shown.

(D) t-SNE plots indicating the expression of representative markers associated with proliferation. See also Figure S4.

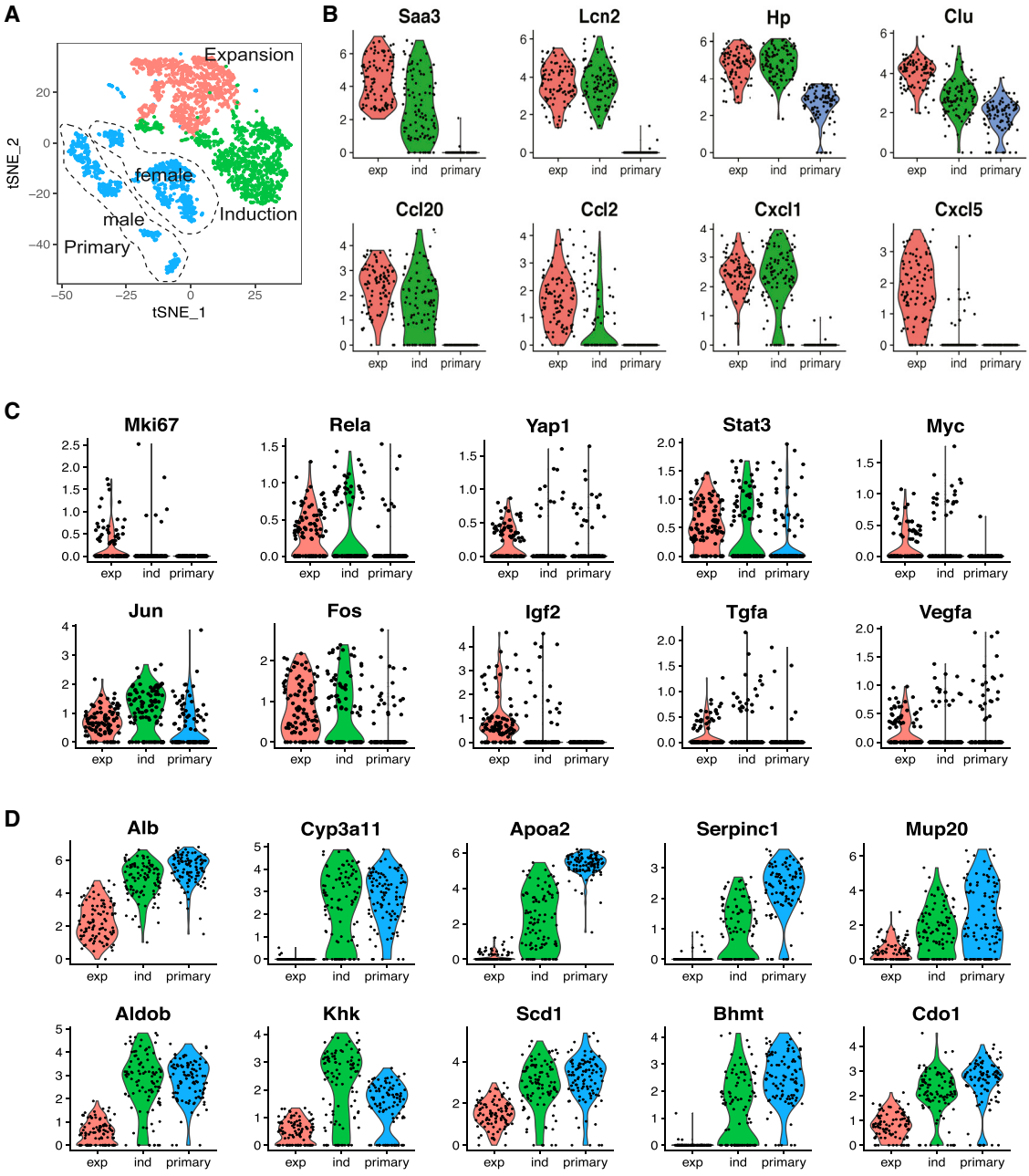

Figure 5. Expression of Inflammation- and Regeneration-Associated Markers in Expansion Medium and Upregulation of Functional Genes in Induction Medium

(A) t-SNE plot of 3D hepatocytes in expansion medium, EGF-induction medium, and primary hepatocytes.

(B) Violin plots of representative differentially expressed genes in hepatocytes cultured in expansion (exp) medium relative to primary hepatocytes, with hepatocytes cultured in induction (ind) medium included for comparison. Differentially expressed genes are determined by Wilcoxon rank-sum test.

(C) Violin plots showing the expression of representative markers associated with regeneration.

(D) Violin plots showing the expression of select genes associated with hepatocyte functions, upregulated in *ind* hepatocytes relative to *exp* hepatocytes, with primary hepatocytes included for comparison. See also Figure S5 for single-cell heatmap.

Clevers, 2016; Michalopoulos, 2007; Su et al., 2015). Notably, transcription factors *Rela* (i.e., NF-κB p65 subunit), *Yap1*, *Stat3*, *Myc*, *Jun*, and *Fos* (which form the AP-1 complex) were detected (Figure 5C). In addition, growth factors that are secreted by hepatocytes *in vivo* that promote proliferation such as *Igf2* and *Tgfa* (Michalopoulos and DeFrances, 1997) and angiogenesis factor *Vegfa* (Shimizu et al., 2001, 2005) were also detected. These data suggest that the mechanisms driving

the expansion of hepatocytes in 3D culture may mimic some aspects of *in vivo* liver regeneration after injury.

In the expansion medium, many serum proteins that are normally expressed in high abundance in the liver were downregulated (Figure S5A), including apolipoproteins (*Apoa2*, *Apoc3*, *Apoc1*), serine protease inhibitors (*Serpin3k*, *Serpin1e*), and major urinary proteins (*Mup3*, *Mup20*, *Mup2*) as well as metabolic cytochrome p450 enzymes (*Cyp3a11*, *Cyp2e1*). We asked whether hepatocyte functional genes could be upregulated in culture. To this end, we compared the gene expression of hepatocytes in expansion medium with 1,245 hepatocytes (derived from one male and one female) cultured in EGF-induction medium (which lacks Wnt and TNFα signals) for the last 4 days of culture. Indeed, upon treatment with EGF-induction medium, many functional genes were promoted (Figure S5B). Notably, *Cyp3a11* and *Alb* were expressed at levels comparable to primary hepatocytes. Other upregulated genes include apolipoproteins *Apoa2* (and related members *Apoc3*, *Apoc1*, *Apoh*), *Serpinc1*, *Mup20*, *Aldob*, *Khk*, *Scd1*, *Bhmt*, and *Cdo1* (Figure 5D). Concomitantly, the expression of ribosomal genes *Rps* and *Rpl,* which are usually high during periods of rapid proliferation (Warner, 1999), were downregulated, along with *Saa3*, *Clu*, *Ccl2*, *Cxcl5*, and *Mki67* (Figures 5B, 5C, and S5B). We also noted the downregulation of regeneration-associated markers, which are now more correlated with expression levels in primary hepatocytes (Figure 5C). Taken together, *in vitro*-expanded hepatocytes maintain their hepatocyte identity, and upon withdrawal of expansion and inflammatory signals, they upregulate suites of genes associated with hepatocyte metabolic functions.

In Vitro Expanded Hepatocytes Engraft *Fah*-Deficient Mice

As a measure of whether *in vitro*-expanded hepatocytes retained functional characteristics, we transplanted these cells into the *Fah*$^{-/-}$ mouse model of liver failure. These mice lack the tyrosine metabolic enzyme *fumarylacetoacetate hydrolase* (*Fah*) and thus model human type 1 tyrosinemia patients that analogously harbor *Fah* mutations (Azuma et al., 2007; Grompe et al., 1993). In *Fah*$^{-/-}$ mice, liver injury can be induced by withdrawal of the hepato-protective drug NTBC. All hepatocyte samples for transplant experiments were transported overnight in suspension in the form of 3D colonies. We reasoned that 3D colonies might promote stability and survival of hepatocytes compared to a single-cell suspension. Approximately 50,000–100,000 colonies were injected intrasplenically as previously described (Azuma et al., 2007). One mouse died 72 days post-transplantation, while the remaining two mice were sacrificed at 103 days after transplant. Immunohistochemistry and immunofluorescence for FAH showed significant engraftment (up to 80%) (Figure 6A), in contrast to the modest (~1%) engraftment that was previously reported upon transplantation of BEC-derived organoids (Huch et al., 2013). FAH+ cells were observed around the CV, PV, and midlobular regions and displayed heterogeneity in cell and nucleus size (Figure 6B).

HNF4α staining was detected in all FAH+ cells as well as host cells (Figure 6C). Engrafted FAH+ cells around the CV expressed pericentral genes such as GLT1, GS, and CYP2E1 (Figures 6D–6F). Notably, the expression of these markers was not detected in host cells (Figures 6D–6F). Engrafted cells also stained for CPS1, whereas host cells expressed low levels of CPS1 (Figure 6G). Of note, engrafted FAH+ cells did not stain for SOX9, KRT7, or KRT19, which mark biliary cells (Figures 6H and S6I), confirming that cultured cells retained hepatocyte identity after transplantation. In a second independent transplant experiment, we injected two mice with 50–100 times fewer cells than used in the first experiment (~1,000 colonies) and one with a single-cell suspension. The livers of transplanted mice were harvested 3–4 months after transplant for analysis. FAH+ cells were detected in all three mice, at up to 2% repopulation (Figure S6A). FAH+ clones as large as 600 μm could be observed; they also expressed functional markers and the proliferation marker KI67 (Figures S6B–S6H).

Next, we asked whether engraftment of cultured hepatocytes and subsequent liver regeneration utilize signals known to promote hepatocyte proliferation during homeostasis, such as the Wnt signaling pathway (Wang et al., 2015). To track Wnt responsiveness in engrafted cells, we first generated 3D hepatocytes from *Axin2-rtTA:TetO-H2B-GFP* donor mice and transplanted the cells into *Fah*$^{-/-}$ mice. Two days before the recipient mice were sacrificed, doxycycline was added to drinking water to induce *Axin2* reporter activity (which tracks Wnt signaling and leads to GFP expression). As expected, hepatocytes around the CVs were GFP+, indicating that they were responding to Wnt signals (Figures S7A and S7B). In addition, GFP+ cells were found at the boundary of FAH+ clones (Figures 7A, S7A, and S7B). In contrast to larger clones that had a clear GFP+ boundary, smaller clones displayed GFP+ cells that were scattered throughout (Figure S7B), suggesting that the FAH− boundary might be a source of Wnt signaling. Consistent with this, GFP+ cells expressed another progenitor marker, the Wnt target gene TBX3 (Figures 7B, S7A, and S7B). TBX3 expression was highest at the clone boundary but was largely absent from the center of the FAH+ clones. Of note, TBX3 expression was also detected at a lower level in host cells, suggesting the presence of a Wnt source outside of FAH+ clones (Figure 7B). KI67 staining revealed proliferation of GFP-expressing cells at the FAH+ nodule boundary (Figure 7C). Some cells that were more centrally located within the engrafted nodules also displayed KI67 staining (Figure S6H).

To query which Wnt family member ligands might regulate the engraftment of the FAH+ cells, we performed mRNA *in situ* hybridization (ISH). *Wnt9b* and *Wnt2* are known to be preferentially expressed in CV endothelial cells, with some expression extending into the lobules (Preziosi et al., 2018; Wang et al., 2015). Consistent with this, we observed *Wnt9b* and *Wnt2* expression in the endothelium of central veins residing in FAH− regions (Figure S7C). In addition, we examined expression of R-spondin family members, as they potentiate Wnt signals in many tissues (de Lau et al., 2014) and *Rspo3* is expressed by the CVs in the liver (Planas-Paz et al., 2016; Rocha et al., 2015). Strikingly, *Rspo3* was highly expressed by vascular structures in FAH− injury zones (Figure S7C) and especially around the periphery of FAH+ clones (Figure 7D). To identify the cell type that expresses *Rspo3*, we performed double ISH. We used *Cd31* (*Pecam1*) to identify endothelial cells and *Cd45* (*Ptprc*) to broadly mark infiltrating and resident immune cells. Double ISH revealed

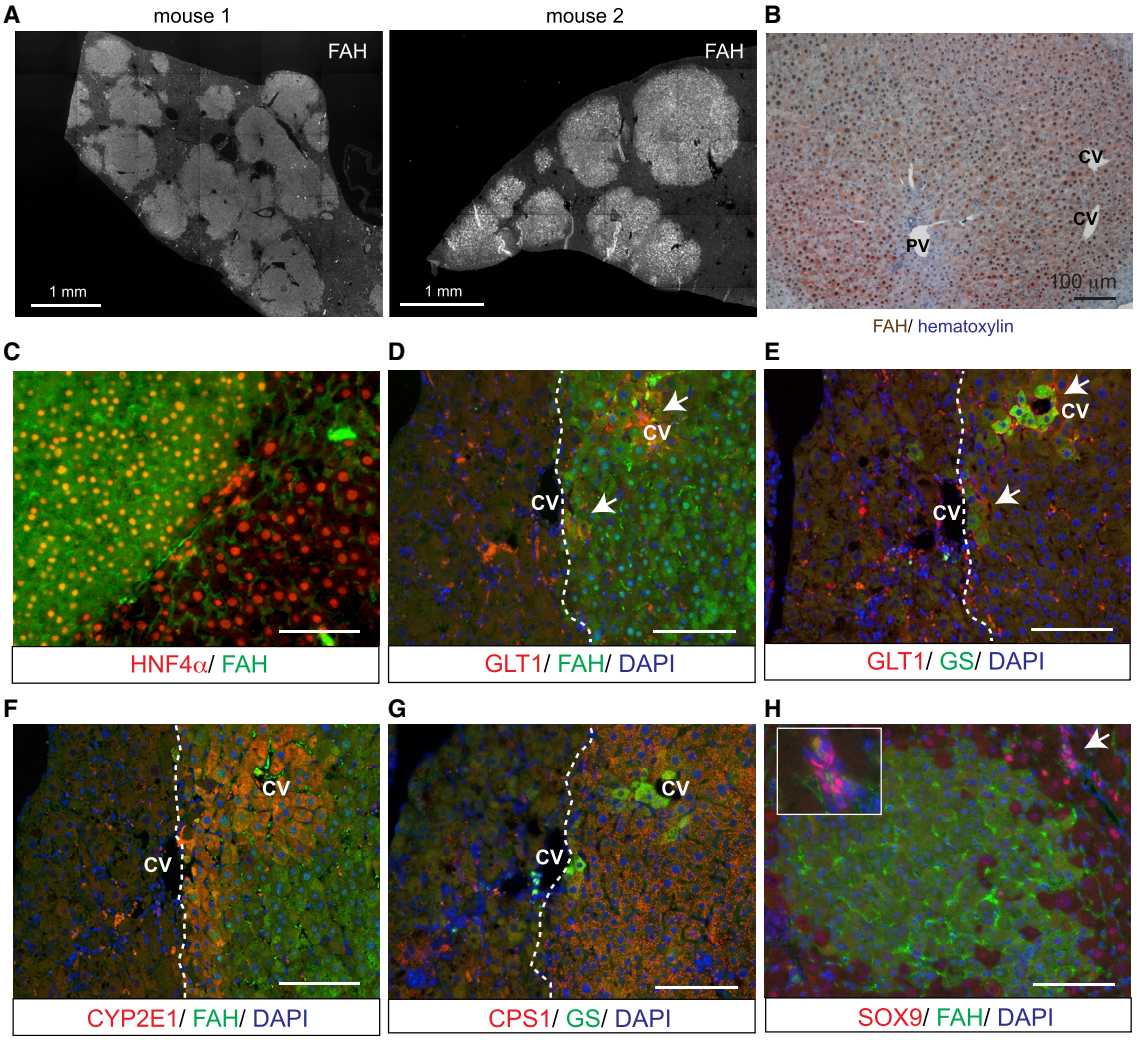

Figure 6. Cultured Hepatocytes Can Engraft in *Fah*-Deficient Mice and Express Hepatocyte Markers

(A) Montage of entire liver sections stained with FAH antibody for two mice are shown. See Figure S6A for additional biological replicates.

(B) Immunohistochemistry for FAH counterstained with hematoxylin, showing a higher-magnification view of engraftment of FAH+ hepatocytes into $Fah^{-/-}$ recipient livers. CV, central vein; PV, portal vein.

(C) Immunofluorescence staining for FAH and the hepatocyte marker HNF4α.

(D–G) Immunofluorescence staining for various markers on serial sections. The dashed line delineates the boundary between FAH+ and FAH− cells. Arrows mark membrane GLT1 staining. CV, central vein.

(H) Immunofluorescence staining for FAH and the biliary marker SOX9 (arrow). Inset, a higher magnification of a nearby bile duct.

Scale bars, 100 μm unless stated otherwise.

that *Rspo3* was expressed in *Cd31*+ endothelial cells but not in clusters of *Cd45*+ cells (Figure S7C).

Among various R-spondin family members, ISH also revealed that *Rspo1* was only found in the liver mesothelium but that two additional Rspo family members, *Rspo2* and *Rspo4*, were found in the liver lobule (Figure S7C). Both *Rspo2* and *Rspo4* localized to dense clusters of cells that morphologically resembled immune cells. They were often found next to vascular structures near FAH+ clones and were distributed in a manner similar to the arrangement of *Cd45*+ cells in FAH− area (Figure S7C). TNFα, known to be secreted by Kupffer cells (Michalopoulos and DeFrances, 1997; Pikarsky et al., 2004), was also found in FAH− regions (Figure S7C). Taken together, our data indicate that 3D hepatocytes can engraft $Fah^{-/-}$ mice, whereupon they continue to express hepatocyte markers, and that cells at the FAH+ clone boundary expand in the presence of WNT-RSPO signals and a regenerative signal-rich environment.

DISCUSSION

The majority of hepatocytes have little proliferative activity in the healthy liver, perhaps explaining challenges in generating long-term cultures from hepatocytes and other difficult-to-expand primary cell types. Our data show that the inflammatory cytokine

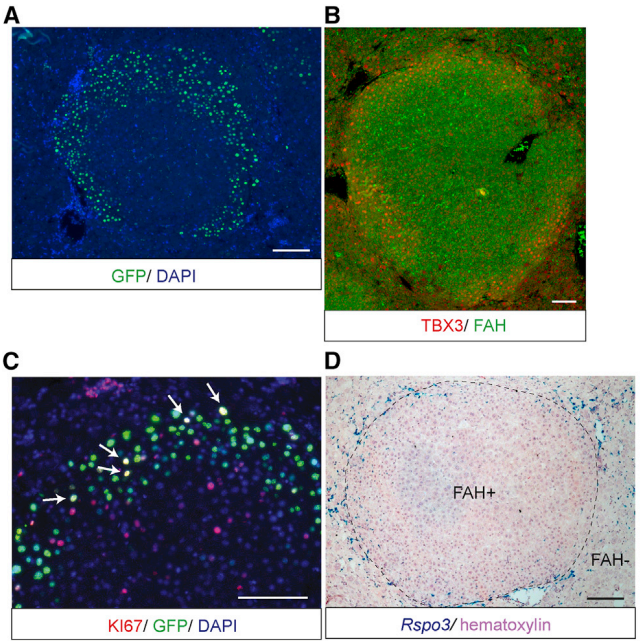

Figure 7. Active Wnt Signaling at the FAH+ Clone Boundary

(A) Wide-field image of an FAH liver section stained for GFP. Donor hepatocytes were derived from Axin2-rtTA:TetO-H2B-GFP mice (see STAR Methods). See also Figure S7A for montages.

(B) Overlay of immunofluorescence staining for TBX3 and FAH.

(C) Overlay of immunofluorescence staining for KI67 and GFP. Arrows mark nuclei that are double positive for both GFP and KI67.

(D) *In situ* hybridization for *Rspo3* counterstained with hematoxylin. Dashed line outlines the FAH+ clone boundary.

Scale bars, 100 μm.

TNFα, in combination with other growth factors and small molecules, enables the long-term culture of primary hepatocytes—which have historically been difficult to expand *in vitro*—while retaining their functionality and engraftment potential. The role of TNFα and cytokines in liver regeneration has been extensively reviewed (Ramadori and Armbrust, 2001; Taub, 2004; Wullaert et al., 2007). *In vitro*, in the absence of TNFα, hepatocyte cultures degenerated within the first 2–3 weeks. Withdrawing TNFα at any point from the culture reduced hepatocyte expansion and resulted in lipid droplet accumulation and eventually deterioration of cells in culture, indicating the continued dependence of the cultures on TNFα for growth. *In vitro*-expanded 3D hepatocytes, upon treatment with induction medium, displayed a variety of functional activities, for instance, albumin secretion, CYP3A11 enzymatic activity, LDL uptake, glycogen storage, and secretion of dye into bile canaliculi, after long-term expansion. Single-cell RNA-seq revealed broad expression of hepatocyte markers and, crucially, the absence of many non-hepatocyte markers. Interestingly, hepatocytes in culture also expressed markers typically associated with liver regeneration and proliferation after partial hepatectomy, suggesting that perhaps the mechanism driving *in vitro* expansion mimics the *in vivo* regeneration process. Upon withdrawal of expansion signals (Wnt and TNFα), many functional genes could be further upregulated, with some genes expressed to levels comparable to primary hepatocytes. It would be worthwhile to investigate whether other cytokines or small molecules can exert similar growth effects on hepatocytes in culture. A manuscript by Hu et al., appearing in this same issue of *Cell* (Hu et al., 2018), describes the culture of mouse and human hepatocytes with a different cocktail of growth factors without TNFα. Interestingly, they found that cell expansion mimics the proliferative response typically observed after liver injury. The authors of this paper also describe extensive differences between hepatocyte organoids and BEC-derived organoids.

Cultured hepatocytes engrafted the livers of *Fah*$^{-/-}$ mice and continued to proliferate *in vivo*, leading to significant liver reconstitution (with up to 80% of the host liver replaced by FAH+ hepatocytes). This is striking, as previous efforts to culture liver cells *in vitro* have led to modest to little engraftment (~1%) in the case of BEC-derived organoids (Huch et al., 2013). The signals driving the *in vivo* proliferation of transplanted hepatocytes remain to be determined but may include inflammatory signals that drive regeneration in other types of injury models, such as partial hepatectomy (Michalopoulos and DeFrances, 1997; Michalopoulos, 2017). We noticed an elevated level of *Wnt* and *Rspo3* expression in the injury area, produced by endothelial cells, as well as *Rspo2*, *Rspo4*, and *Tnfa* produced by infiltrating or resident immune cells. Of note, *Wnt9b* and *Rspo3* produced by the CV induce the proliferation of pericentral hepatocytes during homeostasis (Wang et al., 2015). Indeed, various studies have shown that angiogenesis is a critical aspect for liver regeneration and function *in vivo* (Shimizu et al., 2001, 2005; Taniguchi et al., 2001) and potentially *in vitro* (Camp et al., 2017; Takebe et al., 2013). VEGF secreted by regenerating hepatocytes induces sinusoidal endothelial cell proliferation, and neutralizing VEGF impairs the proliferation of endothelial cells as well as hepatocytes (Taniguchi et al., 2001). These observations suggest that the crosstalk between hepatocytes and endothelial cells, which serve as a major source of WNT and RSPO signals, is essential for liver regeneration.

To capture the complexities associated with such communication between diverse cell types, 3D hepatocyte cultures could eventually provide a more physiologically relevant system to study basic liver biology, model disease, and assess responses to drugs. Indeed, it has been proposed that cells cultured in 3D matrices more closely resemble their *in vivo* counterparts than when cultured in 2D monolayers (Edmondson et al., 2014). For instance, pluripotent stem cell-derived hepatocytes have been aggregated with endothelial and mesenchymal cells to form a "liver bud" (Takebe et al., 2014). Here, we show that 3D hepatocytes derived from primary hepatocytes aggregated readily with HUVECs in culture, and this may in future allow the generation of vascularized mini-livers that could be potentially used for organ transplants. In addition, we demonstrate that 3D hepatocytes could be genetically manipulated by lentiviral infection, and therefore, they may be amenable to other gene editing tools such as CRISPR for correction of faulty genes to treat liver diseases.

Our work, in conjunction with the growing body of evidence for a role of inflammatory cytokines in tissue repair and regeneration, has the potential for application to other organs and disease processes beyond the liver. Regenerative cytokines, such as IL-6, TNFα, and their related family members, have been broadly implicated in wound repair and the healing of

many tissue compartments such as the colon, intestine (Lindemans et al., 2015), gastric tissue (Oguma et al., 2008), hair follicles (Chen et al., 2015), fracture healing (Gerstenfeld et al., 2003), and remyelination by oligodendrocyte progenitors (Arnett et al., 2001). For instance, damaged hair follicles secrete CCl2 to recruit macrophages to the site of injury, which in turn secrete TNFα to activate hair follicle regeneration (Chen et al., 2015), while muscle regeneration is stimulated by macrophage-secreted TNFα (Aurora and Olson, 2014). In addition, IL-22 and IL-6 have been shown to enhance intestinal stem cell proliferation after injury and in *in vitro* culture (Jeffery et al., 2017; Lindemans et al., 2015). More recently, it has been reported that IFN-γ produced by immune cells during parasitic infection induces the expansion of intestinal stem cells with fetal-like phenotypes (Nusse et al., 2018). We propose that harnessing *in vivo* regenerative signals for the *in vitro* expansion of cells in culture may be a powerful approach for manipulating hard-to-expand primary cell types, with a view toward potential applications in regenerative medicine.

STAR★METHODS

Detailed methods are provided in the online version of this paper and include the following:

- KEY RESOURCES TABLE
- CONTACT FOR REAGENT AND RESOURCE SHARING
- EXPERIMENTAL MODEL AND SUBJECT DETAILS
  - Animal Experimental Models
  - Cell lines
- METHOD DETAILS
  - Primary hepatocyte isolation and culture
  - High content imaging
  - Real time quantitative PCR
  - Antibody staining of organoids
  - Functional assays
  - Lentiviral gene delivery
  - Hepatocyte and HUVEC co-culture
  - Single-cell RNA sequencing
  - Transplantation
  - Immunohistochemistry and Immunocytochemistry of engraftment in *Fah*$^{-/-}$ tissues
  - *In Situ* Hybridization
- QUANTIFICATION AND STATISTICAL ANALYSIS
- DATA AND SOFTWARE AVAILABILITY

SUPPLEMENTAL INFORMATION

Supplemental Information includes seven figures and one table and can be found with this article online at https://doi.org/10.1016/j.cell.2018.11.012.

ACKNOWLEDGMENTS

We are grateful to A. Haft, L. Wakefield, and M. Finegold for assistance with transplantation experiments; K. Karlsson for technical assistance with single-cell RNA-seq analysis; K.M. Loh, L.T. Ang, A.J. Sarkar, and E.J. Rulifson for critically reading the manuscript; and the Stanford Functional Genomics Facility for 10x Genomics single-cell library preparation and Genome Sequencing Service Center for 10x Genomics library sequencing. This study was supported by the Howard Hughes Medical Institute (HHMI) and the California Institute for Regenerative Medicine (CIRM); the Genome Sequencing Service Center of the Stanford Center for Genomics and Personalized Medicine Sequencing Center was supported by NIH grant S10OD020141. P.W. is an Ernest and Amelia Gallo Endowed Postdoctoral Fellow supported by the Stanford Child Health Research Institute (CHRI). B.W. is supported by the Burroughs Wellcome Fund Career Awards for Medical Scientists. T.A. is supported by the National Science Foundation (NSF) Graduate Research Fellowship Program.

AUTHOR CONTRIBUTIONS

Conceptualization, W.C.P. and R.N.; Methodology, W.C.P; Investigation, W.C.P, C.Y.L., M.F., F.A., A.Á.-V., T.A., J.Z., P.W., Y.J., B.L., and B.W.; Writing – Original Draft, Reviews & Editing, W.C.P., C.Y.L., T.A., and R.N.; Funding Acquisition, M.G. and R.N.; Resources, M.G. and R.N.; Supervision, R.N.

DECLARATION OF INTERESTS

R.N. is a founder and shareholder of Surrozen and a board member and shareholder of Bio-Techne. M.G. is a co-founder and shareholder of Ambys Medicines. M.G. is also a consultant and shareholder of Yecuris Corp.

Received: May 1, 2018
Revised: August 15, 2018
Accepted: November 12, 2018
Published: November 29, 2018

REFERENCES

Akerman, P., Cote, P., Yang, S.Q., McClain, C., Nelson, S., Bagby, G.J., and Diehl, A.M. (1992). Antibodies to tumor necrosis factor-alpha inhibit liver regeneration after partial hepatectomy. Am. J. Physiol. *263*, G579–G585.

Arnett, H.A., Mason, J., Marino, M., Suzuki, K., Matsushima, G.K., and Ting, J.P. (2001). TNF alpha promotes proliferation of oligodendrocyte progenitors and remyelination. Nat. Neurosci. *4*, 1116–1122.

Ashburner, M., Ball, C.A., Blake, J.A., Botstein, D., Butler, H., Cherry, J.M., Davis, A.P., Dolinski, K., Dwight, S.S., Eppig, J.T., et al.; The Gene Ontology Consortium (2000). Gene ontology: tool for the unification of biology. Nat. Genet. *25*, 25–29.

Aurora, A.B., and Olson, E.N. (2014). Immune modulation of stem cells and regeneration. Cell Stem Cell *15*, 14–25.

Azuma, H., Paulk, N., Ranade, A., Dorrell, C., Al-Dhalimy, M., Ellis, E., Strom, S., Kay, M.A., Finegold, M., and Grompe, M. (2007). Robust expansion of human hepatocytes in Fah-/-/Rag2-/-/Il2rg-/- mice. Nat. Biotechnol. *25*, 903–910.

Beg, A.A., Sha, W.C., Bronson, R.T., Ghosh, S., and Baltimore, D. (1995). Embryonic lethality and liver degeneration in mice lacking the RelA component of NF-kappa B. Nature *376*, 167–170.

Benhamouche, S., Decaens, T., Godard, C., Chambrey, R., Rickman, D.S., Moinard, C., Vasseur-Cognet, M., Kuo, C.J., Kahn, A., Perret, C., and Colnot, S. (2006). Apc tumor suppressor gene is the "zonation-keeper" of mouse liver. Dev. Cell *10*, 759–770.

Borkham-Kamphorst, E., van de Leur, E., Zimmermann, H.W., Karlmark, K.R., Tihaa, L., Haas, U., Tacke, F., Berger, T., Mak, T.W., and Weiskirchen, R. (2013). Protective effects of lipocalin-2 (LCN2) in acute liver injury suggest a novel function in liver homeostasis. Biochim. Biophys. Acta *1832*, 660–673.

Broutier, L., Andersson-Rolf, A., Hindley, C.J., Boj, S.F., Clevers, H., Koo, B.-K., and Huch, M. (2016). Culture and establishment of self-renewing human and mouse adult liver and pancreas 3D organoids and their genetic manipulation. Nat. Protoc. *11*, 1724–1743.

Broutier, L., Mastrogiovanni, G., Verstegen, M.M., Francies, H.E., Gavarró, L.M., Bradshaw, C.R., Allen, G.E., Arnes-Benito, R., Sidorova, O., Gaspersz, M.P., et al. (2017). Human primary liver cancer-derived organoid cultures for disease modeling and drug screening. Nat. Med. *23*, 1424–1435.

Butler, A., Hoffman, P., Smibert, P., Papalexi, E., and Satija, R. (2018). Integrating single-cell transcriptomic data across different conditions, technologies, and species. Nat. Biotechnol. *36*, 411–420.

Camp, J.G., Sekine, K., Gerber, T., Loeffler-Wirth, H., Binder, H., Gac, M., Kanton, S., Kageyama, J., Damm, G., Seehofer, D., et al. (2017). Multilineage communication regulates human liver bud development from pluripotency. Nature *546*, 533–538.

Chen, C.-C., Wang, L., Plikus, M.V., Jiang, T.X., Murray, P.J., Ramos, R., Guerrero-Juarez, C.F., Hughes, M.W., Lee, O.K., Shi, S., et al. (2015). Organ-level quorum sensing directs regeneration in hair stem cell populations. Cell *161*, 277–290.

Clevers, H., Loh, K.M., and Nusse, R. (2014). Stem cell signaling. An integral program for tissue renewal and regeneration: Wnt signaling and stem cell control. Science *346*, 1248012.

Costa, R.H., Kalinichenko, V.V., Holterman, A.-X.L., and Wang, X. (2003). Transcription factors in liver development, differentiation, and regeneration. Hepatology *38*, 1331–1347.

Cressman, D.E., Greenbaum, L.E., DeAngelis, R.A., Ciliberto, G., Furth, E.E., Poli, V., and Taub, R. (1996). Liver failure and defective hepatocyte regeneration in interleukin-6-deficient mice. Science *274*, 1379–1383.

de Lau, W., Peng, W.C., Gros, P., and Clevers, H. (2014). The R-spondin/Lgr5/Rnf43 module: regulator of Wnt signal strength. Genes Dev. *28*, 305–316.

Edmondson, R., Broglie, J.J., Adcock, A.F., and Yang, L. (2014). Three-dimensional cell culture systems and their applications in drug discovery and cell-based biosensors. Assay Drug Dev. Technol. *12*, 207–218.

Gerstenfeld, L.C., Cho, T.J., Kon, T., Aizawa, T., Tsay, A., Fitch, J., Barnes, G.L., Graves, D.T., and Einhorn, T.A. (2003). Impaired fracture healing in the absence of TNF-α signaling: the role of TNF-α in endochondral cartilage resorption. J. Bone Miner. Res. *18*, 1584–1592.

Grompe, M., al-Dhalimy, M., Finegold, M., Ou, C.N., Burlingame, T., Kennaway, N.G., and Soriano, P. (1993). Loss of fumarylacetoacetate hydrolase is responsible for the neonatal hepatic dysfunction phenotype of lethal albino mice. Genes Dev. *7* (12A), 2298–2307.

Hailfinger, S., Jaworski, M., Braeuning, A., Buchmann, A., and Schwarz, M. (2006). Zonal gene expression in murine liver: lessons from tumors. Hepatology *43*, 407–414.

Halpern, K.B., Shenhav, R., Matcovitch-Natan, O., Tóth, B., Lemze, D., Golan, M., Massasa, E.E., Baydatch, S., Landen, S., Moor, A.E., et al. (2017). Single-cell spatial reconstruction reveals global division of labour in the mammalian liver. Nature *542*, 352–356.

Hu, H., Gehart, H., Artegiani, B., Lopez-Iglesias, C., Dekkers, F., Basak, O., van Es, J., Chuva de Sousa Lopes, S.M., Begthel, H., Korving, J., et al. (2018). Long-term expansion of functional mouse and human hepatocytes as 3D organoids. Cell *175*, this issue, 1591–1606.

Hu, Y., Xue, J., Yang, Y., Zhou, X., Qin, C., Zheng, M., Zhu, H., Liu, Y., Liu, W., Lou, G., et al. (2015). Lipocalin 2 Upregulation Protects Hepatocytes from IL1-β-Induced Stress. Cell. Physiol. Biochem. *36*, 753–762.

Huch, M., and Koo, B.-K. (2015). Modeling mouse and human development using organoid cultures. Development *142*, 3113–3125.

Huch, M., Dorrell, C., Boj, S.F., van Es, J.H., Li, V.S.W., van de Wetering, M., Sato, T., Hamer, K., Sasaki, N., Finegold, M.J., et al. (2013). In vitro expansion of single Lgr5+ liver stem cells induced by Wnt-driven regeneration. Nature *494*, 247–250.

Huch, M., Gehart, H., van Boxtel, R., Hamer, K., Blokzijl, F., Verstegen, M.M.A., Ellis, E., van Wenum, M., Fuchs, S.A., de Ligt, J., et al. (2015). Long-term culture of genome-stable bipotent stem cells from adult human liver. Cell *160*, 299–312.

Jeffery, V., Goldson, A.J., Dainty, J.R., Chieppa, M., and Sobolewski, A. (2017). IL-6 Signaling Regulates Small Intestinal Crypt Homeostasis. J. Immunol. *199*, 304–311.

Kang, L.-I., Mars, W.M., and Michalopoulos, G.K. (2012). Signals and cells involved in regulating liver regeneration. Cells *1*, 1261–1292.

Karin, M., and Clevers, H. (2016). Reparative inflammation takes charge of tissue regeneration. Nature *529*, 307–315.

Karin, M., and Greten, F.R. (2005). NF-kappaB: linking inflammation and immunity to cancer development and progression. Nat. Rev. Immunol. *5*, 749–759.

Katsuda, T., Kawamata, M., Hagiwara, K., Takahashi, R.-U., Yamamoto, Y., Camargo, F.D., and Ochiya, T. (2017). Conversion of Terminally Committed Hepatocytes to Culturable Bipotent Progenitor Cells with Regenerative Capacity. Cell Stem Cell *20*, 41–55.

Kietzmann, T. (2017). Metabolic zonation of the liver: The oxygen gradient revisited. Redox Biol. *11*, 622–630.

Kirillova, I., Chaisson, M., and Fausto, N. (1999). Tumor necrosis factor induces DNA replication in hepatic cells through nuclear factor kappaB activation. Cell Growth Differ. *10*, 819–828.

Lee, J., Homma, T., Kurahashi, T., Kang, E.S., and Fujii, J. (2015). Oxidative stress triggers lipid droplet accumulation in primary cultured hepatocytes by activating fatty acid synthesis. Biochem. Biophys. Res. Commun. *464*, 229–235.

Li, B., Dorrell, C., Canaday, P.S., Pelz, C., Haft, A., Finegold, M., and Grompe, M. (2017). Adult Mouse Liver Contains Two Distinct Populations of Cholangiocytes. Stem Cell Reports *9*, 478–489.

Lin, S., Nascimento, E.M., Gajera, C.R., Chen, L., Neuhöfer, P., Garbuzov, A., Wang, S., and Artandi, S.E. (2018). Distributed hepatocytes expressing telomerase repopulate the liver in homeostasis and injury. Nature *556*, 244–248.

Lindemans, C.A., Calafiore, M., Mertelsmann, A.M., O'Connor, M.H., Dudakov, J.A., Jenq, R.R., Velardi, E., Young, L.F., Smith, O.M., Lawrence, G., et al. (2015). Interleukin-22 promotes intestinal-stem-cell-mediated epithelial regeneration. Nature *528*, 560–564.

Lindroos, P.M., Zarnegar, R., and Michalopoulos, G.K. (1991). Hepatocyte growth factor (hepatopoietin A) rapidly increases in plasma before DNA synthesis and liver regeneration stimulated by partial hepatectomy and carbon tetrachloride administration. Hepatology *13*, 743–750.

Magami, Y., Azuma, T., Inokuchi, H., Kokuno, S., Moriyasu, F., Kawai, K., and Hattori, T. (2002). Cell proliferation and renewal of normal hepatocytes and bile duct cells in adult mouse liver. Liver *22*, 419–425.

Michalopoulos, G.K., and DeFrances, M.C. (1997). Liver regeneration. Science *276*, 60–66.

Michalopoulos, G.K. (2007). Liver regeneration. J. Cell. Physiol. *213*, 286–300.

Michalopoulos, G.K. (2017). Hepatostat: Liver regeneration and normal liver tissue maintenance. Hepatology *65*, 1384–1392.

Michalopoulos, G.K., Bowen, W.C., Mulè, K., and Luo, J. (2003). HGF-, EGF-, and dexamethasone-induced gene expression patterns during formation of tissue in hepatic organoid cultures. Gene Expr. *11*, 55–75.

Miyajima, A., Tanaka, M., and Itoh, T. (2014). Stem/progenitor cells in liver development, homeostasis, regeneration, and reprogramming. Cell Stem Cell *14*, 561–574.

Muzumdar, M.D., Tasic, B., Miyamichi, K., Li, L., and Luo, L. (2007). A global double-fluorescent Cre reporter mouse. Genesis *45*, 593–605.

Nusse, Y.M., Savage, A.K., Marangoni, P., Rosendahl-Huber, A.K.M., Landman, T.A., de Sauvage, F.J., Locksley, R.M., and Klein, O.D. (2018). Parasitic helminths induce fetal-like reversion in the intestinal stem cell niche. Nature *559*, 109–113.

Oguma, K., Oshima, H., Aoki, M., Uchio, R., Naka, K., Nakamura, S., Hirao, A., Saya, H., Taketo, M.M., and Oshima, M. (2008). Activated macrophages promote Wnt signalling through tumour necrosis factor-alpha in gastric tumour cells. EMBO J. *27*, 1671–1681.

Overturf, K., Al-Dhalimy, M., Tanguay, R., Brantly, M., Ou, C.N., Finegold, M., and Grompe, M. (1996). Hepatocytes corrected by gene therapy are selected in vivo in a murine model of hereditary tyrosinaemia type I. Nat. Genet. *12*, 266–273.

Pikarsky, E., Porat, R.M., Stein, I., Abramovitch, R., Amit, S., Kasem, S., Gutkovich-Pyest, E., Urieli-Shoval, S., Galun, E., and Ben-Neriah, Y. (2004).

NF-kappaB functions as a tumour promoter in inflammation-associated cancer. Nature *431*, 461–466.

Planas-Paz, L., Orsini, V., Boulter, L., Calabrese, D., Pikiolek, M., Nigsch, F., Xie, Y., Roma, G., Donovan, A., Marti, P., et al. (2016). The RSPO-LGR4/5-ZNRF3/RNF43 module controls liver zonation and size. Nat. Cell Biol. *18*, 467–479.

Preziosi, M., Okabe, H., Poddar, M., Singh, S., and Monga, S.P. (2018). Endothelial Wnts regulate β-catenin signaling in murine liver zonation and regeneration: A sequel to the Wnt-Wnt situation. Hepatol Commun *2*, 845–860.

Ramadori, G., and Armbrust, T. (2001). Cytokines in the liver. Eur. J. Gastroenterol. Hepatol. *13*, 777–784.

Robinson, M.W., Harmon, C., and O'Farrelly, C. (2016). Liver immunology and its role in inflammation and homeostasis. Cell. Mol. Immunol. *13*, 267–276.

Rocha, A.S., Vidal, V., Mertz, M., Kendall, T.J., Charlet, A., Okamoto, H., and Schedl, A. (2015). The Angiocrine Factor Rspondin3 Is a Key Determinant of Liver Zonation. Cell Rep. *13*, 1757–1764.

Schwitalla, S., Fingerle, A.A., Cammareri, P., Nebelsiek, T., Göktuna, S.I., Ziegler, P.K., Canli, O., Heijmans, J., Huels, D.J., Moreaux, G., et al. (2013). Intestinal tumorigenesis initiated by dedifferentiation and acquisition of stem-cell-like properties. Cell *152*, 25–38.

Shimizu, H., Miyazaki, M., Wakabayashi, Y., Mitsuhashi, N., Kato, A., Ito, H., Nakagawa, K., Yoshidome, H., Kataoka, M., and Nakajima, N. (2001). Vascular endothelial growth factor secreted by replicating hepatocytes induces sinusoidal endothelial cell proliferation during regeneration after partial hepatectomy in rats. J. Hepatol. *34*, 683–689.

Shimizu, H., Mitsuhashi, N., Ohtsuka, M., Ito, H., Kimura, F., Ambiru, S., Togawa, A., Yoshidome, H., Kato, A., and Miyazaki, M. (2005). Vascular endothelial growth factor and angiopoietins regulate sinusoidal regeneration and remodeling after partial hepatectomy in rats. World J. Gastroenterol. *11*, 7254–7260.

Skov Olsen, P., Boesby, S., Kirkegaard, P., Therkelsen, K., Almdal, T., Poulsen, S.S., and Nexø, E. (1988). Influence of epidermal growth factor on liver regeneration after partial hepatectomy in rats. Hepatology *8*, 992–996.

Su, T., Bondar, T., Zhou, X., Zhang, C., He, H., and Medzhitov, R. (2015). Two-signal requirement for growth-promoting function of Yap in hepatocytes. eLife *4*. https://doi.org/10.7554/eLife.02948.

Tabula Muris Consortium; Overall coordination; Logistical coordination; Organ collection and processing; Library preparation and sequencing; Computational data analysis; Cell type annotation; Writing group; Supplemental text writing group; Principal investigators (2018). Single-cell transcriptomics of 20 mouse organs creates a Tabula Muris. Nature *562*, 367–372.

Takebe, T., Sekine, K., Enomura, M., Koike, H., Kimura, M., Ogaeri, T., Zhang, R.-R., Ueno, Y., Zheng, Y.-W., Koike, N., et al. (2013). Vascularized and functional human liver from an iPSC-derived organ bud transplant. Nature *499*, 481–484.

Takebe, T., Zhang, R.-R., Koike, H., Kimura, M., Yoshizawa, E., Enomura, M., Koike, N., Sekine, K., and Taniguchi, H. (2014). Generation of a vascularized and functional human liver from an iPSC-derived organ bud transplant. Nat. Protoc. *9*, 396–409.

Taniguchi, E., Sakisaka, S., Matsuo, K., Tanikawa, K., and Sata, M. (2001). Expression and role of vascular endothelial growth factor in liver regeneration after partial hepatectomy in rats. J. Histochem. Cytochem. *49*, 121–130.

Taub, R. (2004). Liver regeneration: from myth to mechanism. Nat Rev Mol Cell Biol. *5*, 836–847.

Torbenson, M., Yang, S.Q., Liu, H.Z., Huang, J., Gage, W., and Diehl, A.M. (2002). STAT-3 overexpression and p21 up-regulation accompany impaired regeneration of fatty livers. Am. J. Pathol. *161*, 155–161.

van Amerongen, R., Bowman, A.N., and Nusse, R. (2012). Developmental stage and time dictate the fate of Wnt/β-catenin-responsive stem cells in the mammary gland. Cell Stem Cell *11*, 387–400.

Wang, B., Zhao, L., Fish, M., Logan, C.Y., and Nusse, R. (2015). Self-renewing diploid Axin2(+) cells fuel homeostatic renewal of the liver. Nature *524*, 180–185.

Warner, J.R. (1999). The economics of ribosome biosynthesis in yeast. Trends Biochem. Sci. *24*, 437–440.

Webber, E.M., Bruix, J., Pierce, R.H., and Fausto, N. (1998). Tumor necrosis factor primes hepatocytes for DNA replication in the rat. Hepatology *28*, 1226–1234.

Wullaert, A., van Loo, G., Heyninck, K., and Beyaert, R. (2007). Hepatic tumor necrosis factor signaling and nuclear factor-kappaB: effects on liver homeostasis and beyond. Endocr. Rev. *28*, 365–386.

Yamada, Y., Kirillova, I., Peschon, J.J., and Fausto, N. (1997). Initiation of liver growth by tumor necrosis factor: deficient liver regeneration in mice lacking type I tumor necrosis factor receptor. Proc. Natl. Acad. Sci. USA *94*, 1441–1446.

Yamada, Y., Webber, E.M., Kirillova, I., Peschon, J.J., and Fausto, N. (1998). Analysis of liver regeneration in mice lacking type 1 or type 2 tumor necrosis factor receptor: requirement for type 1 but not type 2 receptor. Hepatology *28*, 959–970.

Yimlamai, D., Christodoulou, C., Galli, G.G., Yanger, K., Pepe-Mooney, B., Gurung, B., Shrestha, K., Cahan, P., Stanger, B.Z., and Camargo, F.D. (2014). Hippo pathway activity influences liver cell fate. Cell *157*, 1324–1338.

Yu, H.-M.I., Liu, B., Costantini, F., and Hsu, W. (2007). Impaired neural development caused by inducible expression of Axin in transgenic mice. Mech. Dev. *124*, 146–156.

Zheng, G.X.Y., Terry, J.M., Belgrader, P., Ryvkin, P., Bent, Z.W., Wilson, R., Ziraldo, S.B., Wheeler, T.D., McDermott, G.P., Zhu, J., et al. (2017). Massively parallel digital transcriptional profiling of single cells. Nat. Commun. *8*, 14049.

STAR★METHODS

KEY RESOURCES TABLE

REAGENT or RESOURCE	SOURCE	IDENTIFIER
Antibodies		
Rabbit Polyclonal anti-CPS1	Abcam	Cat# Ab3682; RRID: AB_304000
Rabbit Polyclonal anti- Cytochrome P450 2E1 (CYP2E1)	Abcam	Cat# Ab28146; RRID: AB_2089985
Goat Polyclonal anti-DPPIV/CD26	R&D systems	Cat# AF954; RRID: AB_355739
Mouse Monoclonal anti-FAA(FAH)	ABM	Cat# Y123010; RRID: AB_2752242
Rabbit Polyclonal anti-FAH	M Grompe's lab	Cat# FAH OR026; RRID: AB_2752243
Rabbit Polyclonal anti-GLT1	Frontier Institute	Cat# GLT1-Rb-Af670; RRID: AB_2571718
Mouse Monoclonal anti-GS (Clone GS-6)	Millipore	Cat#MAB302; RRID: AB_2110656
Rabbit Polyclonal anti- Hnf4α (Clone H-171)	Santa Cruz Biotechnology	Cat#SC-8987; RRID: AB_2116913
Mouse Monoclonal anti- Hnf4α (Clone K9218)	Abcam	Cat# Ab41898; RRID: AB_732976
Rat Monoclonal anti- Ki67 (SolA15)	eBioscience	Cat#14-5698-82; RRID: AB_10854564
Rabbit Polyclonal anti-KRT7 (CK7)	Millipore	Cat# HPA007272; RRID: AB_1079181
Rabbit anti-CK19 (KRT19)	AbboMax	Cat# 602-670
Rabbit polyclonal anti- NF-kB p65 (phospho S536)	Abcam	Cat#ab86299; RRID: AB_1925243
Rabbit Polyclonal anti- Sox9	Millipore	Cat# AB5535; RRID: AB_2239761
Goat Polyclonal anti-TBX3 (Clone A-20)	Santa Cruz Biotechnology	Cat#SC-17871; RRID: AB_661666
Rabbit polyclonal anti-YAP	Cell Signaling Technology	Cat#4912S; RRID: AB_2218911
Rabbit polyclonal anti-GFP	Abcam	Cat#13970; RRID: AB_300798
Donkey anti Goat Biotin-SP-AffiniPure	Jackson ImmunoResearch	Cat# 705-065-147; RRID: AB_2340397
Chemicals, Peptides, and Recombinant Proteins		
Liver Perfusion Medium	Invitrogen	17701-038
Collagenase type IV	Wellington	LS004188
HBSS with Ca Mg	GIBCO	24020117
100 μm strainer	Falcon	352360
24 gauge 3/4 inch angiocatheter	BD	381700
Percoll Plus	Sigma	E0414-250mL
Matrigel GF reduced	BD	356231
William's E media	GIBCO	A1217601
Glutamax	GIBCO	35050-061
Non-Essential Amino Acids	GIBCO	11140-050
Penicillin/streptomycin	GIBCO	15140-122
Normocin	Invivogen	ant-nr-2
B27 supplement	GIBCO	17504-044
N2 supplement	GIBCO	17502048
Nicotinamide	Sigma-Aldrich	N0636
N-acetylcysteine	Sigma-Aldrich	A9165
Y27632	Peprotech	1293823
A83-01	Tocris	2939
CHIR 99021	Peprotech	2520691
EGF	Peprotech	AF-100-15
HGF	Peprotech	100-39-100
TNFα	Peprotech	315-01A
Noggin	Peprotech	250-38

(*Continued on next page*)

Continued

REAGENT or RESOURCE	SOURCE	IDENTIFIER
Dexamethasone	Tocris	1126
Dispase	Stem Cell Technologies	07913
IL-6	Peprotech	216-16
TrypLE Express	GIBCO	12605010
Bambanker	Wako	50-999-554
Luciferin-IPA	Promega	V9001
Fluorescein diacetate	Santa Cruz Biotechnology	sc-294598
Trypsin-EDTA	GIBCO	25200056
DMEM	Thermo	11965092
HSC LipidTOX	Invitrogen	H34475
Reserpine	Sigma Aldrich	R0875-1G
Hoechst 33342	Life Technologies	H3570
DAPI	Thermo Scientific	D1306
NTBC	Yecuris	20-0026
Critical Commercial Assays		
RNAscope 2.5 HD Reagent Kit-Red	Advanced Cell Diagnostics	Cat# 322360
RNAscope 2.5 HD Duplex Reagent Kit	Advanced Cell Diagnostics	Cat# 322430
RNeasy mini kit	QIAGEN	74104
High Capacity cDNA Reverse Transcription kit	Life Technologies	4368814
Mouse albumin ELISA kit	Assaypro	EMA2201-1
LDL Uptake Assay kit	Abcam	ab1331267
Periodic Acid-Schiff kit	Sigma Aldrich	395B-1KT
Deposited Data		
Single-cell RNA-seq dataset	This paper.	GEO: GSE120067
Experimental Models: Cell Lines		
HEK293T	ATCC	CRL-1573
HepG2	ATCC	HB-8065
GFP-expressing human umbilical vein endothelial cells (GFP-HUVECs)	Angioproteomie	cAP-0001GFP
Experimental Models: Organisms/Strains		
C57BL/6J	Jackson lab	000664
Axin2-CreERT2	Jackson lab	018867
Axin2-rtTA	Jackson lab	016997
Rosa26-mT/mG	Jackson lab	007676
TetO-H2B-GFP	Jackson lab	005104
Oligonucleotides		
RNAscope Probe: Mm-Fah-C2 (target region: 490-1364)	Advanced Cell Diagnostics	Cat#503431-C2
RNAscope Probe: Mm-Wnt9b (target region: 706-1637)	Advanced Cell Diagnostics	Cat#405091
RNAscope Probe: Mm-Wnt2 (target region: 857-2086)	Advanced Cell Diagnostics	Cat#313601
RNAscope Probe: Mm-Rspo3 (target region: 731-2164)	Advanced Cell Diagnostics	Cat#402011
RNAscope Probe: Mm-Rspo 1 (target region: 550-1679)	Advanced Cell Diagnostics	Cat#401991
RNAscope Probe: Mm-Rspo2 (target region: 537-1452)	Advanced Cell Diagnostics	Cat# 402001
RNAscope Probe: Mm-Rspo4 (target region: 1180-2202)	Advanced Cell Diagnostics	Cat#402021
RNAscope Probe: Mm-CD31/Pecam1-C2 (target region: 915-1827)	Advanced Cell Diagnostics	Cat#316721-C2
RNAscope Probe: Mm-CD45/Ptprc-C2 (target region: 2922-3866)	Advanced Cell Diagnostics	Cat# 318651-C2
RNAscope Probe: Mm-TNFa (target region: 41-1587)	Advanced Cell Diagnostics	Cat# 311081
See Table S1 for Taqman qPCR probes.		

(*Continued on next page*)

Continued

REAGENT or RESOURCE	SOURCE	IDENTIFIER
Recombinant DNA		
Plasmid: pLKO.1-puro-CMV-TurboGFP	Sigma Aldrich	SHC003
Plasmid: psPAX2	Addgene	12260
Plasmid: pMD2.g	Addgene	12259
Software and Algorithms		
Prism Graphpad 7.0	Graphpad software	https://www.graphpad.com
Adobe Photoshop CC 2018	Adobe	https://www.adobe.com/product/photoshop.html
Adobe Illustrator CC 2018	Adobe	https://www.adobe.com/product/illustrator.html
ImageJ	NIH	https://imagej.nih.gov/ij/
Cell Ranger version 2.1.1	10x Genomics	https://support.10xgenomics.com/single-cell-gene-expression/software/downloads/latest
Seurat R Package	Butler et al., 2018	https://satijalab.org/seurat
HCS Studio Cell Analysis Software	Thermo Fisher	https://www.thermofisher.com

CONTACT FOR REAGENT AND RESOURCE SHARING

Further information and requests for resources and reagents should be directed to and will be fulfilled by the Lead Contact, Roel Nusse (rnusse@stanford.edu).

EXPERIMENTAL MODEL AND SUBJECT DETAILS

Animal Experimental Models

The Institutional Animal Care and Use Committee at Stanford University approved all animal methods and experiments. Animal transplantation was conducted in accordance with the Institutional Review Committee at Oregon Health and Science University. Wild-type C57BL/6J mice, Axin2-CreERT2 (B6.129(Cg)-Axin2 $^{tm1(cre/ERT2)Rnu}$/J) (van Amerongen et al., 2012), Rosa26-mT/mG (B6.129(Cg)-Gt(ROSA)26Sor $^{tm4(ACTB-tdTomato,-EGFP)Luo}$/J (Muzumdar et al., 2007), Axin2-rtTA (B6.Cg-Tg(Axin2-rtTA2S*M2)7Cos/J) and TetO-H2B-GFP (Tg(tetO-HIST1H2BJ/GFP)47Efu/J) (Yu et al., 2007) were obtained from The Jackson Laboratory (JAX). Axin2-CreERT2:Rosa26-mT/mG mice were derived by crossing male heterozygous Axin2-CreERT2 with homozygous female Rosa26-mT/mG mice. Axin2-rtTA:TetO-H2B-GFP mice were derived by crossing either male or female heterozygous Axin2-rtTA mice with heterozygous TetO-H2B-GFP mice. *Fah*$^{-/-}$ mice (*Fah* $^{\Delta exon5}$) (Overturf et al., 1996) were maintained on a C57BL/6J background (JAX) and 6-8 week old male and female mice were used for transplantation studies. All *Fah*$^{-/-}$ mice were treated with 2-(2-nitro-4-trifluoromethylbenzoyl)-1,3-cyclohexanedione (NTBC) in drinking water at a concentration of 8 mg/ml. All mice were housed with a 12-h light/dark cycle with *ad libitum* access to water and normal chow.

Cell lines

HepG2 and HEK293T cell lines were obtained from ATCC. HepG2 is a human cell line derived from liver cancer from a 15 year-old Caucasian. HepG2 was cultured in RPMI 1641 with GlutaMax (GIBCO), supplemented with 10% fetal bovine serum (FBS; Omega Scientific) with antibiotic/antimycotic (GIBCO, penicillin 100U/ml, streptomycin 100 ug/ml, amphotericin B 0.25 ug/ml). 293T is a human cell line derived from the HEK293 female embryonic kidney cell line, transformed with the SV40 large T antigen. 293T was cultured in DMEM supplemented with 10% (v/v) FBS (Omega Scientific), 2 mM Glutamax (GIBCO), 0.1 mM non-essential amino acids (GIBCO), penicillin 100 U/ml (GIBCO) and streptomycin 10 μg/ml (GIBCO). GFP-expressing human umbilical vein endothelial cells (GFP-HUVECs), derived from pooled HUVECs, were obtained from Angio-Proteomie (Boston, MA) and cultured according to manufacturer's instructions. Briefly, GFP-HUVECs were expanded on a Geltrex-coated (Life Technologies) 6-well plate in EGM-2 Bullet kit medium (Lonza) supplemented with normocin (Invivogen) and trypsinized prior to co-culture experiments. Cell lines were kept in culture for no more than 10 passages after being obtained from the manufacturers. All cells were maintained at 37°C at 5 – 7% CO_2 humidified air.

METHOD DETAILS

Primary hepatocyte isolation and culture

Hepatocytes were isolated by a two-step collagenase perfusion technique with modifications. Briefly, the inferior vena cava (IVC) was cannulated with a 24-gauge 3/4-inch angiocatheter (BD) and the portal vein was cut. The liver was perfused via the IVC with 100 mL of Liver Perfusion Medium (Invitrogen) at 37°C, followed by perfusion with 100 mL of collagenase type IV (Wellington) in Hank's Balanced Salt Solution (HBSS, containing calcium and magnesium; GIBCO). After the liver was digested, it was dissected out and cut into small pieces and passed through a 100 μm strainer (Falcon). Hepatocytes were separated from non-parenchymal cells (NPCs) by low-speed centrifugation (50 g x 5 mins x 3, brake = 2), and further purified by Percoll gradient centrifugation (50% v/v, Sigma).

For 3D culture, hepatocytes were embedded in growth-factor reduced (GFR) matrigel (BD), at approximately 1000 cells per 20 μL of matrigel droplets. William's E medium containing 1% (v/v) Glutamax, 1% (v/v) Non-Essential Amino Acids, 1% (v/v) penicillin/streptomycin (all from GIBCO), 0.2% (v/v) normocin (Invivogen), 2% (v/v) B27 (GIBCO), 1% (v/v) N2 supplement (GIBCO), 10 mM nicotinamide (Sigma-Aldrich), 1.25 mM N-acetylcysteine (Sigma-Aldrich), 10 μM Y27632 (Peprotech), 1 μM A83-01 (Tocris) was used as the basal medium. Expansion medium contained 3 μM CHIR99021 (Peprotech), 25 ng/mL EGF (Peprotech), 50 ng/mL HGF (Peprotech) and 100 ng/mL TNFα (Peprotech). Media was replaced every 2 – 3 days. After approximately 2 weeks in culture, matrigel was digested with dispase (Stem Cell Technologies), and released intact organoids were embedded in new matrigel droplets and cultured for another one to two weeks. Of note, hepatocyte organoids were not dissociated by dispase. From the second passage onward, after dispase digestion of matrigel, released organoids were further incubated with TrypLE Express (GIBCO) for 5 – 10 minutes at 37°C. Then, 3D colonies were broken up into multiple-cell aggregates by gentle pipetting. To ensure high viability of hepatocytes, prolonged enzyme incubation or mechanical dissociation that resulted in single-cell suspension was avoided. Dissociated cell aggregates were embedded in matrigel at appropriate densities (usually at 500 – 2000 cells per 20 μL drops). Remaining cells were frozen in Bambanker (Wako) at −80°C and could be thawed following standard procedures for subsequent cultures.

For long term culture, media was supplemented with 50 ng/mL noggin (Peprotech) for at least 4 – 7 days of culture from the second passage onward. Cultures were typically passaged every 14 – 20 days, when the size of organoids was > 200 – 300 μm, or when the matrigel droplets were overcrowded. For culture without TNFα, the cytokine was omitted from the medium, but otherwise contained all other factors present in the standard expansion medium. For culture with IL-6, 50 ng/ml IL-6 was used in the expansion medium without TNFα. For hepatocyte differentiation, hepatocytes were cultured in expansion medium for approximately 2 weeks, and then switched to differentiation medium for the last 3 – 5 days of culture. EGF- induction medium contained 25 ng/ml EGF, 50 ng/ml HGF and 3 μM dexamethasone (DEX) (Tocris), and Wnt- induction medium contained 3 μM CHIR 99021 and 3 μM DEX, in the basal medium described above.

High content imaging

The CellInsight CX7 High-Content Screening (HCS) Platform (Thermo Fisher Scientific) was used for colony counting and nuclear intensity measurements. Briefly, cultures were incubated with medium containing 10 μg/mL Hoechst 33342, (Life Technologies), 5 μM reserpine (Sigma-Aldrich), 1:250 dilution of HCS LipidTOX (Invitrogen) for 30 – 60 minutes in the presence of 50% (v/v) dispase. 3D organoids were released from matrigel by gentle pipetting, washed twice with medium and then transferred to a 96-well plate (Corning) for imaging. The colonies were imaged on wide-field, confocal z stack, and bright-field and were quantified using HCS Studio Cell Analysis Software (Thermo Fisher). Cell debris or dead cells were excluded based on colony size, nuclear intensity and length-to-width ratio, and the same threshold was applied in each experiment for the colony counting of hepatocytes cultured with or without TNFα.

Real time quantitative PCR

3D colonies were harvested from matrigel using dispase and total RNA was purified using the RNeasy mini kit (QIAGEN) according to the manufacturer's instructions. The total RNA was reverse-transcribed using random primers (High Capacity cDNA Reverse Transcription kit, Life Technologies). Gene expression was assayed by real-time PCR using TaqMan Gene Expression Assays (Applied Biosystems) on an ABI 7900HT real-time PCR system. GAPDH was used as an internal control for the amount of RNA input in each well. Taqman™ qPCR probes used are listed in Table S1. Measurements were performed in triplicate for each biological sample.

Antibody staining of organoids

For whole-mount organoid staining, organoids were fixed in 2% paraformaldehyde at 4°C overnight, washed 3x in PBS and then placed in PBS-Tw (PBS, 10% v/v NDS, 0.1% v/v Tween) for 30 minutes in glass staining dishes. Primary antibody was applied to organoids at 1:20 (v/v) dilution in PBS-Tw. Organoids were incubated overnight at 4°C and then washed 3x in PBS-Tw. Secondary antibodies were applied in PBS-Tw for 1 hour followed by 3 washes in PBS-Tw. Hoechst or DAPI was added to stain nuclei before visualization. Organoids were imaged on a Zeiss Cell Observer SD spinning disk microscope. Images were processed using Photoshop. All antibodies used are listed in Key Resources Table.

Functional assays

Albumin secretion assay was performed using the mouse albumin ELISA kit (Assaypro) according to the manufacturer's instructions. Briefly, hepatocytes in expansion medium (3, 5, and 7 months) were switched to EGF- or Wnt- induction media during the last 4 – 6 days of culture. Culture media was harvested for measurements two days after the last media change. Freshly isolated adult primary hepatocytes from two mice (50,000 cells) were plated on a 2D collagen-coated plate in EGF- induction medium and media was harvested 4 days later for measurements. CYP3A11 activity was measured using the P450-Glo^{TM} CYP3A4 assay system according to the manufacturer's instructions. Hepatocytes in expansion medium were switched to EGF- or Wnt- induction media for the last 4 – 6 days of culture. 3D colonies and control cells, HepG2 and HEK293T (both cultured in 2D monolayer), were incubated with 3 μM of luciferin-IPA in 200 μL of RPMI (10% v/v FBS) overnight for the measurement of CYP3A11 activity. To evaluate LDL uptake, hepatocytes in EGF- induction medium were incubated overnight with LDL conjugated with DyLight^{TM}-550 (LDL Uptake Assay Kit, Abcam). For visualization of LDL uptake, 3D colonies in matrigel were treated with dispase to release intact organoids and excess dyes were removed with 3 washes. To assess secretion into bile canaliculi, hepatocytes in EGF- induction medium were incubated with fluorescein diacetate (Santa Cruz Biotechnology) for 15 – 30 min at 37°C, and fluorescent dye was replaced with culture media and visualized immediately. To evaluate glycogen storage, 3D colonies in expansion medium were embedded in paraffin section and stained using a Periodic Acid-Schiff kit (Sigma Aldrich) according to the manufacturer's instructions. Negative control slides were treated with human saliva containing α-amylase.

Lentiviral gene delivery

At 24 hours prior to transfection, HEK293T cells were plated in a 6-well plate at 8 × 10^5 cells per well in DMEM (10% v/v FBS). Cells growing at ~70%–80% confluency were transfected with 1 μg of pLKO.1-puro-CMV-TurboGFP (Sigma Aldrich) along with 2nd generation lentiviral packaging and envelope plasmids, 0.75 μg of psPAX2 and 0.25 μg of pMD2.g (gifts from D. Trono, Addgene #12260, #12259). At 36 hours post transfection, the media containing lentiviral particles was collected and passed through a 0.45 μm filter. Polybrene was added to a final concentration of 4 μg/mL. 3D hepatocyte colonies released from matrigel were resuspended in expansion or EGF-induction media in ultra-low attachment plates for lentiviral infection. The filtered media containing lentivirus was added at a 1:1 (v/v) dilution to target hepatocyte organoids. A second infection was performed at 24 hours post-infection. GFP expression was visualized at 48 hours after the first infection. For visualization of hepatocytes in 2D monolayer, hepatocytes were transitioned to geltrex-coated 2D culture in expansion medium (2% v/v FBS) at day 5 post-second infection, and imaged 2 days later on a Leica DMI 600B microscope.

Hepatocyte and HUVEC co-culture

For hepatocyte and HUVEC co-culture experiments, 3D hepatocyte organoids (in the order of hundreds) were resuspended with GFP-HUVECs on a 96-well (10,000 – 20,000 cells) or 24-well (60,000 cells) flat bottom ultra-low attachment plates (Corning) at a 1:1 (v/v) dilution of hepatocyte expansion and HUVEC media and cultured for approximately 2 weeks.

Single-cell RNA sequencing

Single-cell RNA sequencing was performed using the 10x Genomics Chromium System (Zheng et al., 2017). Hepatocytes were derived from one male and one female mouse, cultured for a total of 75 and 97 days, respectively. Briefly, after passaging, hepatocytes were cultured in expansion medium for 12 days (termed 'expansion': 3 μM CHIR 99021, 25 ng/mL EGF, 50 ng/mL HGF and 100 ng/mL TNFα) or switched to EGF- induction medium (termed 'induction': 25 ng/mL EGF, 50 ng/mL HGF and 3 μM DEX) for the last 4 days of culture (i.e., day 9–12). To obtain a single-cell suspension, the cultures were incubated with dispase for 20 minutes, washed twice with William's E medium and further incubated with 0.25% Trypsin-EDTA solution (GIBCO) for 30 minutes. The organoids were then gently dissociated by mechanical pipetting, washed twice with William's E medium to remove cell debris and then flow through a 40 μm strainer to remove cell aggregates. Cell counts were performed using the Cellometer K2 (Nexelcom). We pooled together the cells from one male and one female and loaded a total of ~1,200 cells from each culture condition on the Chromium Instrument (10x Genomics, Pleasanton, CA, USA).

Single-cell RNA-seq library was generated using GemCode Single-Cell 3′ Gel Bead and Library V2 Kit. Single-cell library was loaded on an Illumina HiSeq 4000 System with 2 × 100 paired-end kits with the following reads: 26 bases Read 1 (cell barcode and unique molecular identifier (UMI)), 8 bases i7 Index 1 (sample index) and 98 bases Read 2 (transcript). The Cell Ranger Software (Version 2.1.1) was used to perform sample de-multiplexing, barcode processing and 3′ UMI counting. For 'expansion' culture, approximately 1,208 cells were sequenced, with the mean reads of 243, 654 per cell and median genes of 3,832 per cell, median UMI counts of 22,969 per cell. For 'induction' culture, approximately 1275 cells were sequenced, with the mean reads of 43,292 per cell and median genes of 1986 per cell, median UMI counts of 6,686 per cell. Datasets for 3-month old primary hepatocytes (termed 'primary'), derived from two female and one male, were obtained from GEO database with the accession numbers GSM3040892, GSM3040898 and GSM3040899, and was previously described here (Tabula Muris Consortium et al., 2018). Data obtained from the GEO database was reprocessed using Cell Ranger version 2.1.1 with mm10 as the reference genome. Single-cell data was analyzed using the standard workflow on the Seurat R Package (Butler et al., 2018). Female-derived cells could be distinguished from male-derived cells based on *Xist* gene expression. Cells that had at least one UMI for the *Xist* gene were assigned as female cells, while the remaining were assigned as male cells. For the analysis of the 'expansion' dataset, the gene-barcode matrix

was filtered based on the number of genes detected per cell (< 200 genes/cell excluded) and percent.mito (> 25% excluded), and genes that were expressed in fewer than 10 cells were excluded. For the joint-analysis of 'expansion', 'induction' and primary hepatocytes, cells with < 500 or > 6000 genes/cells and > 25% percent.mito were excluded. After filtering, we obtained 1,192 cells from expansion medium (592 male, 600 female) and 1,245 cells from induction medium (811 male, 434 female). These cells were analyzed by PCA, and the top 10 principal components were selected based on the elbow plot for downstream clustering analysis. t-SNE plots were used to visualize the clusters. The list of most highly expressed genes and their average UMI counts were obtained using the Seurat R Package. Differentially expressed genes (DEGs) between different population of the hepatocytes were determined using the Wilcoxon rank sum test implemented in Seurat R Package, with min.pct = 0.25. Gene ontology analysis was performed using the Gene Ontology Consortium web platform described previously (Ashburner et al., 2000).

Transplantation

Hepatocytes were derived from 8-week old mice of wild-type or *Axin2-rtTA:TetO-H2B-GFP* background (Wang et al., 2015). In the first experiment, hepatocytes derived from three mice were cultured in expansion medium for 17-, 17- and 21- days, respectively. In the second experiment, hepatocytes derived from three mice were expanded for 48-, 55- and 105- days, respectively. For transplantation, intact organoids were released from matrigel by dispase treatment. 3D organoids were resuspended in expansion medium supplemented with 2% (v/v) FBS (Omega Scientific) and transported overnight on ice for transplantation. Transplantation was performed according to a previously described protocol (Azuma et al., 2007; Li et al., 2017). One day before transplantation, *Fah*$^{-/-}$ mice were taken off NTBC. 3D organoids were injected intra-splenically the following day. In the first experiment, mice were put on five NTBC ON cycles (first cycle: 8 d off, 3 d on; second cycle: 7 d off, 5 d on; third cycle: 16 d off, 5 d on; fourth cycle: 7 d off, 4 d on; fifth cycle: 21 d off, 3 d on; final 25 d off). In the second experiment, mice were put on three NTBC cycles (first cycle: 14 d off, 7 d on; second cycle: 14 d off, 4 d on; third cycle: 21 d off, 3 d on; final 21 d off) or four cycles (first cycle: 8 d off, 4 d on; second cycle: 14 d off, 4 d on; third cycle: 21 d off, 3 d on; fourth cycle: 24 d off, 4 d on; final 33 d or 44 d off). The livers of transplanted mice were harvested at various time points after transplantation and evaluated by FAH antibody staining. FAH engraftment area was determined using ImageJ.

Immunohistochemistry and Immunocytochemistry of engraftment in *Fah*$^{-/-}$ tissues

Liver samples were isolated from *Fah*$^{-/-}$ hosts, fixed in 10% neutral buffered formalin pH 7.4 overnight and processed for embedding in paraffin. 5 μm sections were cut, de-paraffinized and re-hydrated by standard methods and processed for further staining. Immunohistochemistry to detect FAH in liver samples was performed using standard methods (Azuma et al., 2007; Li et al., 2017). For immunofluorescence staining, Citrate or Tris-based antigen retrieval (Vector Labs) was performed on de-paraffinized sections. Slides to be stained with anti-TBX3 antibody were treated with Biotin/Avidin Blocking reagent (Vector labs). All slides were blocked in 10% (v/v) NDS PBS-Tw and then incubated in primary antibodies for 1 hour at room temperature or overnight at 4°C. Samples stained for TBX3 were incubated with biotinylated secondary antibody followed by incubation with Streptavidin-647. Other slides were incubated in secondary antibodies against the respective primary antibody host for 1 hour at room temperature. Slides were washed and mounted using ProlongGold with DAPI (Invitrogen) for visualization. Samples were imaged using a Zeiss Imager Z.2, Zeiss Cell Observer SD spinning disk microscope or a CellInsight CX7 High-Content Screening (HCS) Platform (Thermo Fisher Scientific).

In Situ Hybridization

Paraffin-embedded tissue sections were cut at 5 μm thickness and processed for detection of mRNA using the manual RNAscope 2.5 HD Assay-Red or RNAscope 2.5 HD Duplex Kits (Advanced Cell Diagnostics, Hayward CA) according to the manufacturer's instructions. Images were taken at 10x and 20x magnification on a Zeiss Imager Z.2. Images were processed using Photoshop. Probes used are listed in Key Resources Table.

QUANTIFICATION AND STATISTICAL ANALYSIS

Statistical comparisons in Figure 1D were carried out using the non-parametric Mann-Whitney U test, with the following significance: ns = $p > 0.05$, * = $p \leq 0.05$, ** = $p \leq 0.01$, *** = $p \leq 0.001$, **** = $p \leq 0.0001$. Graphpad prism 7.0 was used to perform statistical analyses and to generate graphs.

DATA AND SOFTWARE AVAILABILITY

Single-cell RNA-seq dataset (10x Genomics Chromium System) are deposited in GEO database with the accession number GEO: GSE120067.

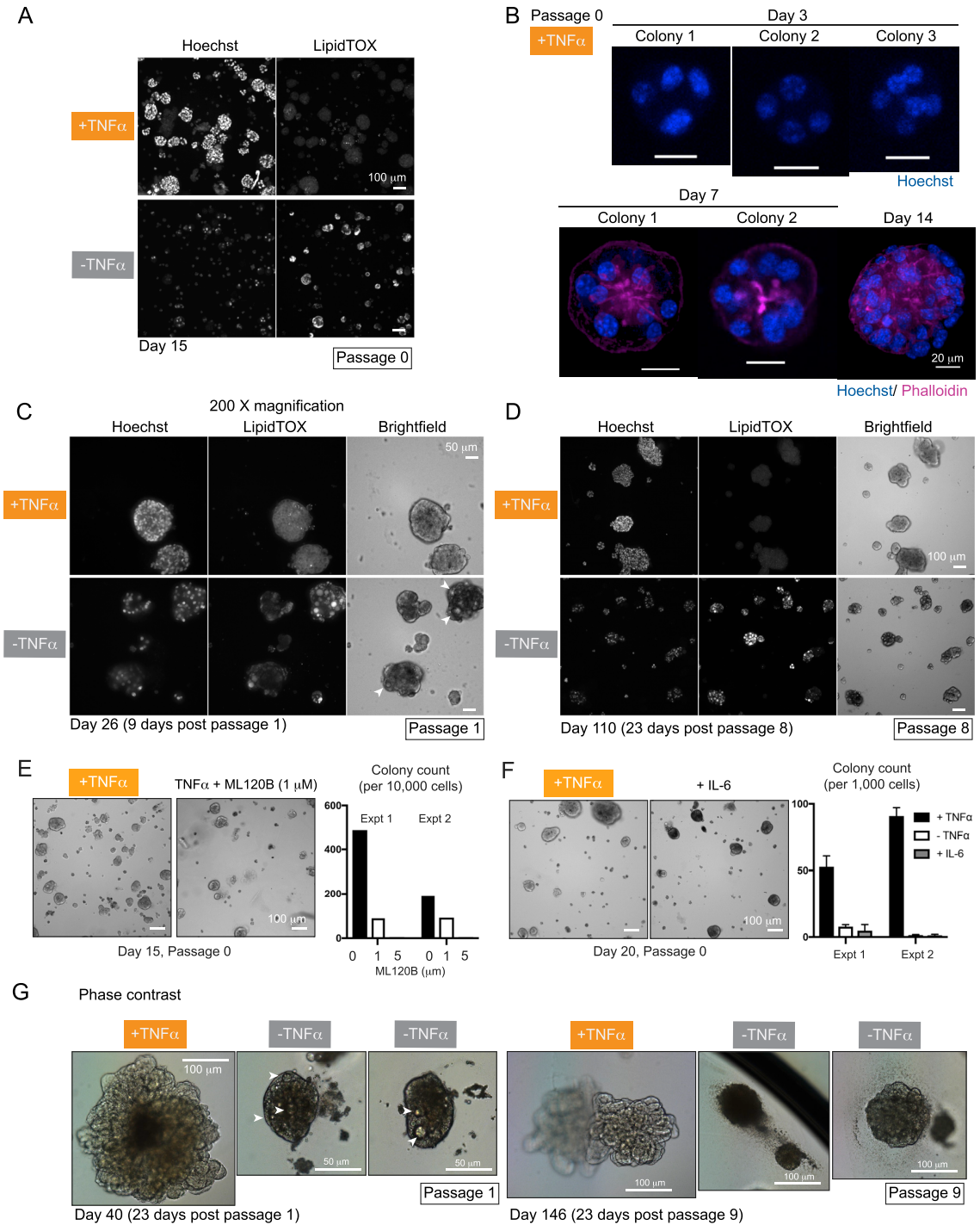

Figure S1. Hepatocyte Expansion Is Dependent on TNFα, Related to Figure 1

(A) Freshly isolated primary mouse hepatocytes cultured with or without TNFα for 2 weeks at passage 0. Nuclei (Hoechst) and lipid droplets (LipidTOX) are shown. Corresponding brightfield images are shown in Figure 1A.

(B) Colony expansion of hepatocytes in the presence of TNFα for the first 14 days of culture, stained for Hoechst alone or Hoechst and Phalloidin. Representative images of multiple colonies are shown. Scale bars, 20 μm.

(C) Higher magnifications of Hoechst- or LipidTOX-stained and brightfield images of hepatocyte cultures at passage 1. Data are from the same experiment shown in Figure 1C. After 17 days in culture, cells were passaged and TNFα was either maintained or withdrawn from culture media. The total number of days in culture, and the number of days after passaging are indicated. Arrowheads indicate lipid droplets.

(D) Images of cultured hepatocytes corresponding to the samples shown in Figure 1D. At passage 8, TNFα was either maintained or withdrawn from culture media.

(legend continued on next page)

(E) Primary hepatocytes were cultured with TNFα in the absence or presence of IKKβ inhibitor ML120B. ML120B was added to the culture on day 7 after plating and colony counts were performed on day 15, n = 2 biological replicates.
(F) Primary hepatocytes were cultured with or without TNFα, or with IL-6 and colonies were counted on day 20. Mean and SD of three measurements are shown, n = 2 biological replicates.
(G) Phase-contrast images of cultures at early and late passages. TNFα was either maintained or withdrawn from culture media at indicated passage numbers. Arrowheads indicate lipid droplets.

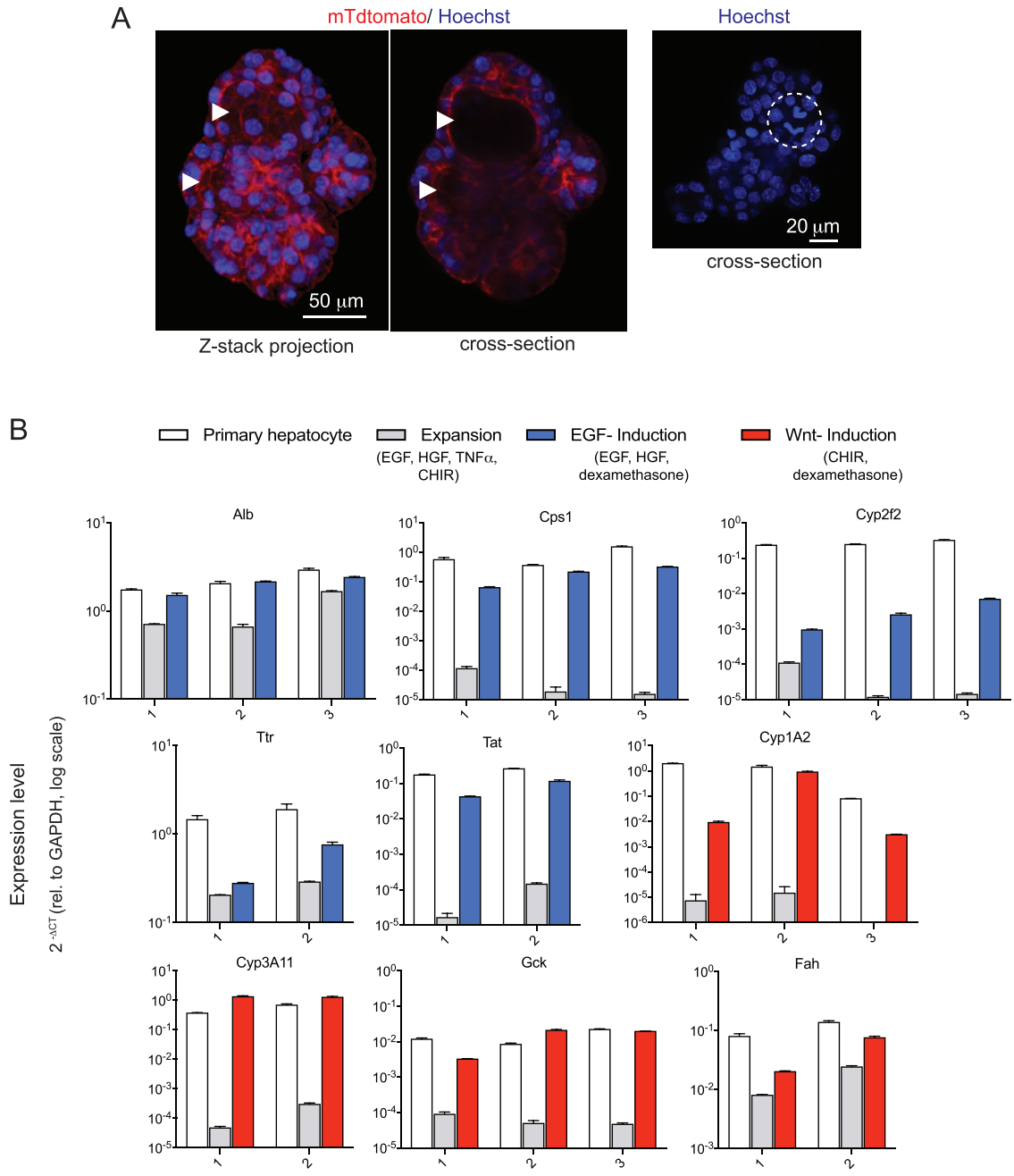

Figure S2. Expression and Modulation of Functional Markers in 3D Hepatocytes, Related to Figure 2

(A) Confocal images of 3D hepatocytes showing the presence of lumens within the organoid (arrowheads; left). Mitotic cell observed by Hoechst stain (dashed circle; right).

(B) Gene expression analysis by qPCR. Data are represented as mean and SD of three independent measurements for each biological replicate. Data are an extension of Figure 2.

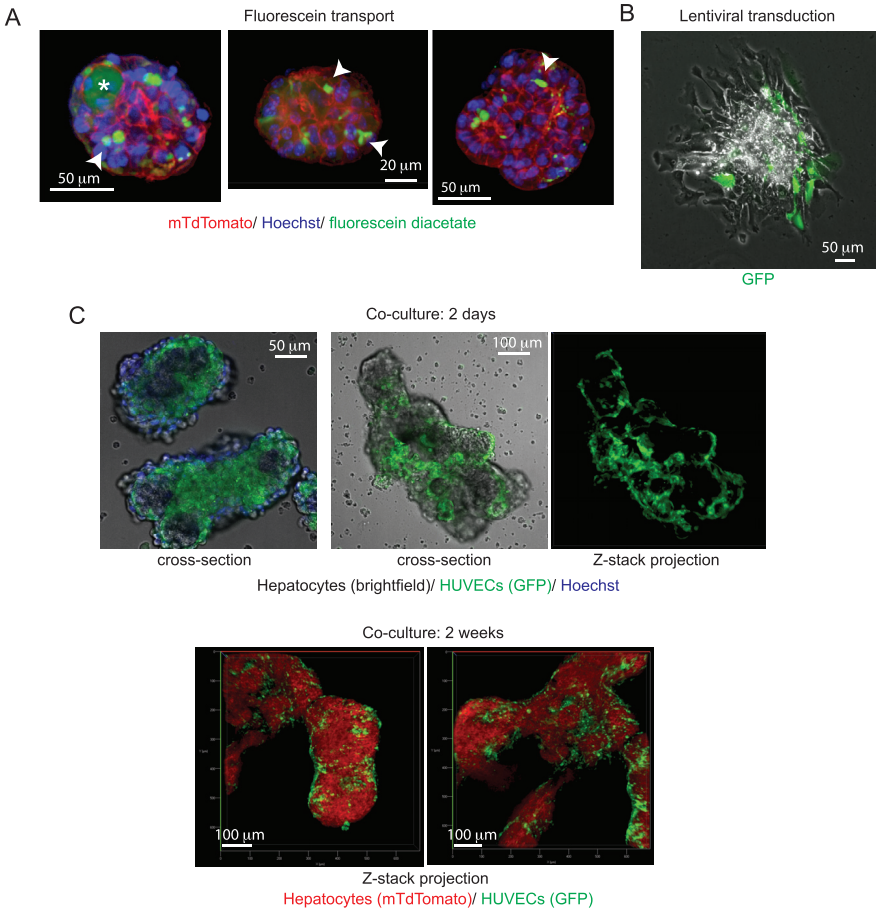

Figure S3. 3D Hepatocytes Perform Hepatocyte Functions, Related to Figure 3

(A) Confocal images (z stack projection) of multiple hepatocyte colonies, showing fluorescein diacetate (green) accumulation in the bile canaliculi structures (arrowheads) and lumen (asterisk).

(B) Overlay of brightfield and fluorescence images of a representative lentivirus-infected hepatocyte colony. At day 5 after a second lentiviral infection, 3D colonies were transferred from ultra-low attachment plates to geltrex coated plates, and imaged 2 days later.

(C) Aggregates of 3D hepatocyte colonies with GFP-HUVECs, two days (top) and two weeks (bottom) after the initiation of co-culture.

A

Most highly expressed genes.

Hepatocyte cluster		Cycling cluster	
Gene	**Average UMI Count**	**Gene**	**Average UMI Count**
Saa3	164.378128	Saa3	166.0180942
Trf	150.695845	*Hp*	155.3277778
Hp	148.7346806	*Trf*	152.9247886
Serpina1b	119.1100786	*Serpina1b*	90.37273952
Fth1	78.81929922	*Fth1*	79.49640466
Serpina1c	76.35391094	*Ftl1*	67.50884942
Clu	74.82216109	*Serpina1c*	65.49558114
Eef1a1	73.5691673	*Clu*	62.84534754
Ftl1	70.9810032	*C3*	61.63317383
Serpina1a	68.06863974	*Eef1a1*	61.31086761
C3	60.97453664	*Serpina1a*	58.45737314
Tpt1	59.27271049	*Tpt1*	50.08528738
Apoa1	57.78576988	*Guca2b*	49.49464814
Lcn2	57.09410685	*Hpx*	49.36115697
Hpx	51.57912563	*Lcn2*	48.6795465
Guca2b	43.14290974	*Fau*	33.55911784
Ahsg	43.01078839	*Apoe*	31.86147924
Fau	38.95311867	*Ahsg*	31.83645319
Apoe	33.61268908	*Tmsb10*	25.89474732
Tmsb10	29.2156167	*Malat1*	24.7715845

Single-cell heatmap of the most enriched genes in the cycling cluster.

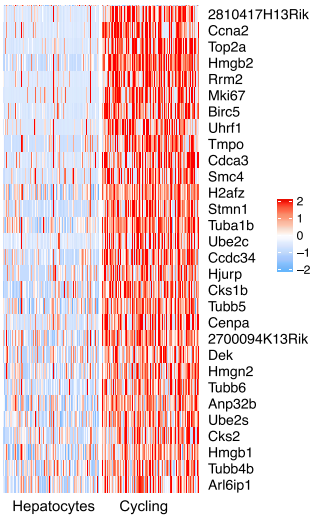

B

Gene ontology analysis

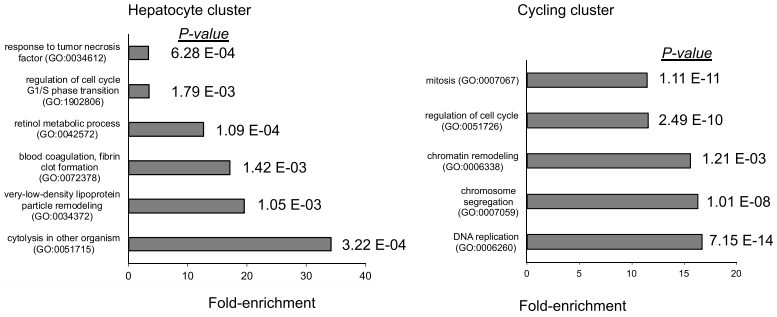

Figure S4. Single-Cell RNA-Seq Reveals Broad Expression of Hepatocyte Markers and the Presence of a Subset of Cycling Cells, Related to Figure 4

(A) A list of the 20 most highly expressed genes in the hepatocyte and cycling clusters and their average unique molecular identifier (UMI) counts (left). Mitochondrial and ribosomal genes are omitted for clarity. Single-cell heatmap showing the 30 most differentially expressed genes in the cycling cluster (right). Differentially expressed genes are determined by the Wilcoxon rank sum test.

(B) GO term analysis for the 500 most highly expressed genes in the hepatocyte cluster (left) and the 150 most differentially expressed genes in the cycling cluster (right).

Figure S5. Expression of Regeneration-Associated Markers in Expansion Medium and Upregulation of Functional Genes in Induction Medium, Related to Figure 5

(A) Single-cell expression heatmap of differentially expressed genes for hepatocytes in expansion medium (exp) relative to primary hepatocytes, showing the most upregulated and downregulated genes. Mitochondrial and ribosomal genes are omitted for clarity.

(B) Single-cell expression heatmap of differentially expressed genes for hepatocytes in EGF- induction medium (ind) relative to expansion medium (exp), showing the most upregulated and downregulated genes. Primary hepatocytes are included for comparison.

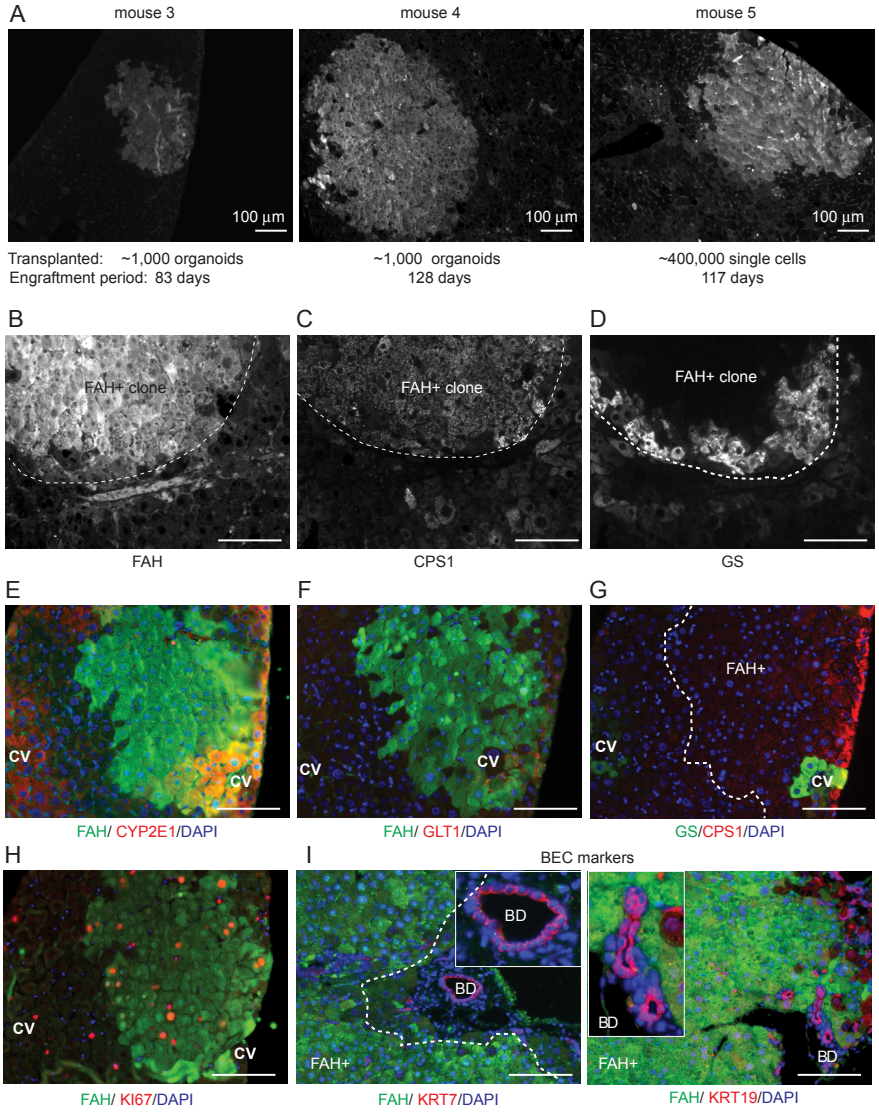

Figure S6. Cultured Hepatocytes Can Engraft in *Fah*-Deficient Mice and Express Hepatocyte Markers, Related to Figure 6

(A) Liver sections from three biological replicates stained with FAH antibody. Number of colonies or cells transplanted, and length of engraftment are indicated.
(B–D) Immunofluorescence staining for (B) FAH, (C) CPS1, (D) GS on serial sections. Dashed line demarcates the boundary between FAH+ and FAH- cells.
(E–H) Immunofluorescence images of co-staining for various markers on serial sections. Dashed line demarcates the boundary between FAH+ and FAH- cells. CV, central vein.
(I) Immunofluorescence staining for FAH and the biliary markers KRT7 and KRT19. Inset, a higher magnification of nearby bile ducts (BD).
Scale bars, 100 μm.

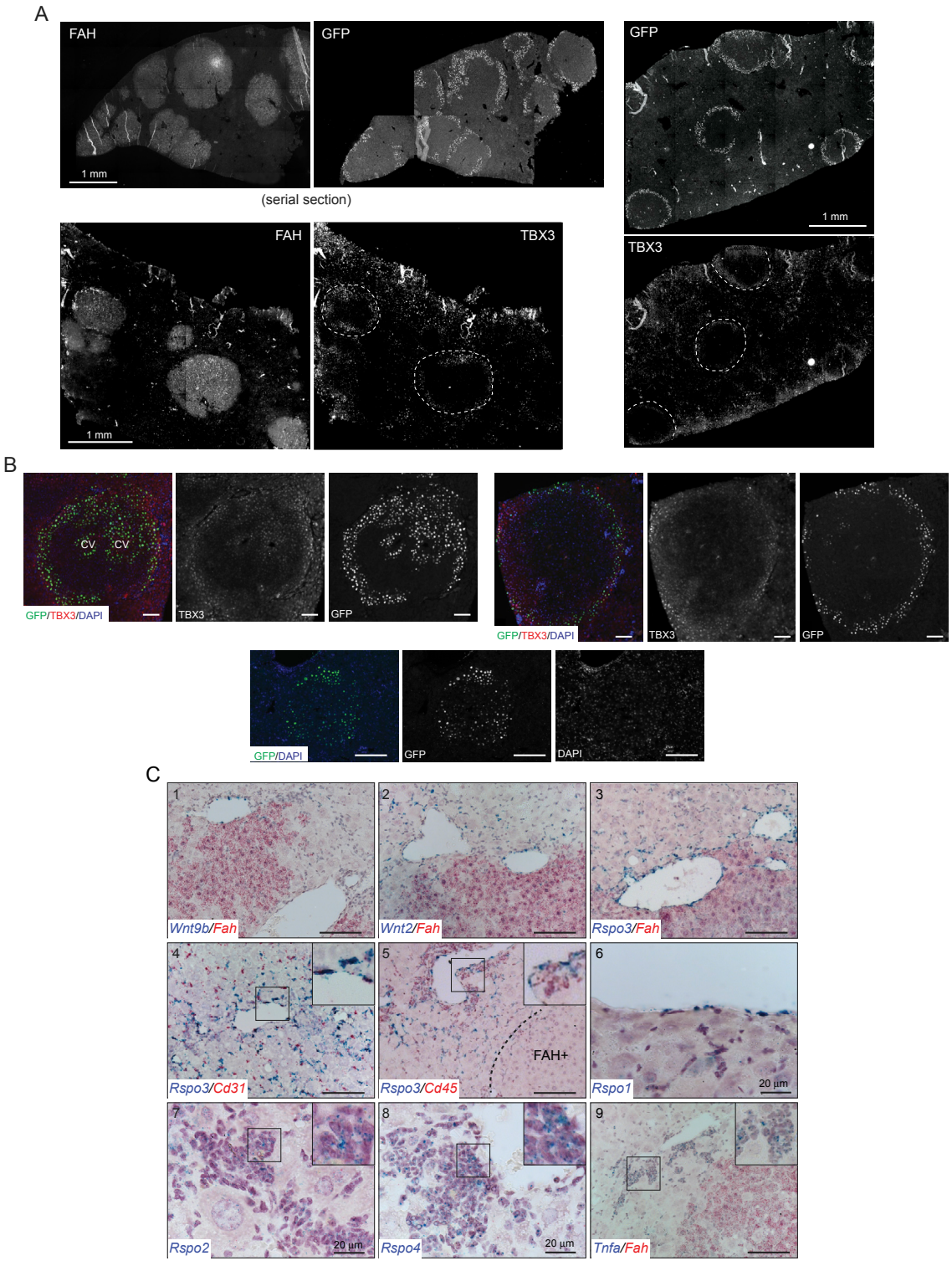

Figure S7. Active Wnt Signaling at the FAH+ Clone Boundary, Related to Figure 7

(A) Wide-field montage of an entire liver section stained for FAH and GFP (serial section, also shown in Figure 6A), FAH-TBX3 (co-staining) and GFP-TBX3 (co-staining). Dashed line outlines the FAH clone boundary. Donor hepatocytes were derived from Axin2-rtTA:TetO-H2B-GFP mice (see STAR Methods).

(B) A higher magnification of representative FAH clones stained for TBX3 and GFP or GFP alone. CV, central veins. Scale bars, 100 μm.

(legend continued on next page)

(C) *In situ* hybridization to follow expression of Wnt pathway components and injury signals in FAH- liver tissue. (1-5,9) Dual-color *in situ* hybridization (red and blue signals) counterstained with hematoxylin (light purple stain). (6-8) Single-color *in situ* hybridization (blue signal) counterstained with hematoxylin (light purple stain). (1) *Wnt9b* is expressed around central veins in FAH- host livers. (2) *Wnt2* is similarly expressed near central veins and in pericentral sinusoidal endothelial cells. (3-8) *In situ* hybridization to localize the expression of Rspo family members. (3) *Rspo3* is highly expressed in central veins. Expression also extends to sinusoids. (4) CV-associated *Rspo3* positive cells express the endothelial cell marker *Cd31/Pecam*. Inset represents a higher magnification of CV endothelial cells. (5) *Rspo3* transcripts do not co-localize with *Cd45*. Inset shows a dense cluster of cells positive for the *Cd45* signal that does not overlap with *Rspo3*. FAH+ clone boundary is marked with a dashed line. (6) *Rspo1* is not expressed in the liver but is found in the mesothelial layer surrounding the liver. (7) *Rspo2* is found in dense clusters of cells interspersed among FAH- hepatocytes. Inset shows a close-up view of transcript localization. (8) *Rspo4* is found in dense clusters of cells that often reside near vascular structures. Inset shows *Rspo4* signal at higher magnification. (9) *Tnfa* is expressed in dense clusters of cells that are found near the vasculature. Inset shows a higher magnification view of transcript localization to these cells. Scale bars, 100 μm, unless stated otherwise.